Dendritic cells enter lymph vessels by hyaluronan-mediated docking to the endothelial receptor LYVE-1

Louise A. Johnson[1], Suneale Banerji[1], William Lawrance[1], Uzi Gileadi[1], Gennaro Prota[1], Kayla A. Holder[1], Yaowaluck M. Roshorm[2], Tomáš Hanke[3,4], Vincenzo Cerundolo[1], Nicholas W. Gale[5], David G. Jackson[1]

[1]MRC Human Immunology Unit, University of Oxford, Weatherall Institute of Molecular Medicine, John Radcliffe Hospital, Headington, Oxford, OX3 9DS, U.K. [2]King Monkut's University of Technology, Thonburi, Thailand. [3]The Jenner Institute, University of Oxford, Old Road Campus Research Building, Roosevelt Drive, Oxford, OX3 7DQ, U.K. [5]Regeneron Pharmaceuticals, Tarrytown, NY, USA.

Correspondence should be addressed to D. G. J. (david.jackson@imm.ox.ac.uk) or L.A.J. (louise.johnson@imm.ox.ac.uk)

Abstract

Trafficking of tissue dendritic cells (DCs) *via* lymph is critical for generating cellular immune responses in draining lymph nodes. Here, we showed that DCs docked to the basolateral surface of lymphatic vessels and transited to the lumen through hyaluronan-mediated interactions with the lymph-specific endothelial receptor LYVE-1, in dynamic transmigratory cup-like structures. Furthermore, we showed that targeted *Lyve1* gene deletion, antibody blockade or depletion of the DC hyaluronan coat not only delayed lymphatic trafficking of dermal DCs but also blunted their capacity to prime $CD8^+$ T-cell responses in skin-draining lymph nodes. Our findings uncovered a previously unknown function for LYVE-1 and showed that transit through the lymphatic network was initiated by recognition of leukocyte-derived hyaluronan.

Introduction

Afferent lymphatic vessels provide essential conduits for transporting antigen-presenting dendritic cells (DCs), from the periphery to draining lymph nodes (LNs). During normal homeostasis, low level trafficking of immature tissue resident DCs allows for local immune surveillance, whereas in inflammation and infection, the enhanced migration of both resident and monocyte-derived DCs allows for efficient generation of primary immune responses to invading pathogens[1].

The first key steps in this chain of events are migration of DCs within the tissue interstitium towards initial lymphatic capillaries, transit across endothelium into the vessel lumen, and crawling in the direction of downstream lymphatic collectors[2]. These processes are directed by a combination of interstitial flow[3], chemotaxis and haptotaxis in response to gradients of lymphatic endothelial-derived chemokines including CCL21, CXCL12 and CX3CL1 that engage with their cognate leukocyte receptors CCR7, CXCR4 and CX3CR1[4–11] and semaphorins[12]. However, the mechanisms underlying DC transit across lymphatic endothelium are poorly understood.

It is now appreciated that initial lymphatic capillaries have specialized inter-endothelial junctions distinct from those of blood capillaries[13]. These comprise loose, overlapping flaps anchored on their sides by "buttons" containing the adherens junction molecule VE-cadherin and tight junction-associated proteins such as claudins and ZO-1. Notably, the openings formed by these flaps constitute 1 – 2 μm valve-like portals that are just large enough for migrating leukocytes to enter. Indeed, endogenous class II Major Histocompatibility Complex positive ($MHCII^+$) DCs have been observed to squeeze through such junctions into lymphatic capillaries[13]. Nevertheless, the interactions between DCs and lymphatic endothelium that facilitate transit remain unknown. Previous studies have reported transit does not involve

conventional integrin-based adhesion and is instead mediated through contractile forces[5,14], whereas others have shown that in inflammation, transit requires engagement of DC integrins with their endothelial ligands ICAM-1 and VCAM-1[15–17]. Several other candidate adhesion molecules have also been reported to regulate DC entry to the lymphatics, including CD31, CD99, CD137, L1CAM, ALCAM and the scavenger receptors CLEVER-1 and Mannose receptor[9,18,19]. However, these are also expressed in blood vessel endothelium and no adhesion molecules specific to lymphatic entry have been convincingly described.

One particularly abundant component of button-like lymphatic junctions that has been proposed to mediate leukocyte entry is the lymphatic vessel endothelial protein LYVE-1, a receptor for the large ubiquitous glycosaminoglycan polymer hyaluronan (HA), [GlcNAcβ1-4GlcUAβ1-3]n[20]. LYVE-1 is present at high density within the distinctive overlapping junctions of initial lymphatics but largely absent from the conventional tight junctions of larger collector vessels. Furthermore, LYVE-1 is closely related to the primary leukocyte HA receptor CD44, which mediates HA-dependent adhesion and extravasation of leukocytes across inflamed blood vessels[21].

Here we have explored the involvement of LYVE-1 and its ligand HA in the trafficking of leukocytes within lymphatic vessels. Using *Lyve1*$^{-/-}$ mice and function-blocking mAbs, we showed that efficient lymphatic trafficking of DCs from the inflamed skin was dependent upon LYVE-1, and that LYVE-1-HA interactions mediated an initial vessel entry step that was rate-limiting for DC-primed immune responses in draining lymph nodes. Moreover, we demonstrate that migrating DCs assembled an endogenous HA surface coat, which enabled docking to the lymphatic endothelium *via* LYVE-1 within discrete transmigratory cups that enveloped the transiting DC and facilitated its passage to the vessel lumen. These findings identify an important immunological function for this widely used lymphatic marker and

reveal a previously unidentified role for the LYVE-1-HA interaction, as a regulator of leukocyte trafficking in the lymphatics.

Results

Lyve1 gene deletion impairs DC migration to skin-draining LNs

To explore the involvement of LYVE-1 in the migration of DCs from the peripheral tissues to lymph during both normal homeostasis and inflammation, we used a mouse skin contact-hypersensitivity model, in which sensitization with the chemical allergen oxazolone induces rapid mobilization of epidermal Langerhans cells and dermal DCs, and subsequent trafficking to skin-draining LNs that is detectable within 24 h (**Supplementary Fig. 1a**)[22]. We found a reduction in the numbers of skin-derived $CD11c^+FITC^+$ DCs recovered in draining inguinal and axillary LNs at 6 h and 24 h post oxazolone-sensitization in *Lyve1*$^{-/-}$ BALB/c mice compared to *Lyve1*$^{+/+}$ littermates, which was followed by a compensatory rise in $CD11c^+FITC^+$ DC numbers arriving at LNs at 48 h in the *Lyve1*$^{-/-}$ BALB/c mice (**Fig. 1a**). This interruption in trafficking was highly reproducible and appeared to affect all subsets of migratory $CD11c^+MHCII^+$ $FITC^+$ DCs, including $CD11b^+$ DCs, $CD103^+$ DCs, $EpCAM^+$ DCs and $Langerin^+$ DCs (**Supplementary Fig. 1b-c**). The composition of leukocyte populations in the LNs of unchallenged *Lyve1*$^{-/-}$ and *Lyve1*$^{+/+}$ BALB/c mice was almost identical (**Supplementary Fig 2**), indicating a defect in inflammation-associated trafficking, rather than the steady-state composition of LNs in the *Lyve1*$^{-/-}$ mice. We also observed a less marked, but statistically significant reduction in DC accumulation in LNs at 6h post oxazolone-sensitization and a similar, non-significant trend at 24 h in *Lyve1*$^{-/-}$ C57BL/6 mice compared to *Lyve1*$^{+/+}$ littermates together with a rebound at 48h post-sensitization (**Supplementary Fig. 3a-c**), in contrast to the original analysis of *Lyve1*$^{-/-}$ C57BL/6 mice, which failed to detect a migration defect[23], probably due to the incomplete nature of those initial studies. However, similar to the original analysis[23], we detected no obvious differences in gross lymphatic vessel or junctional ultrastructure in *Lyve1*$^{-/-}$ mice compared to *Lyve1*$^{+/+}$

littermates on either background. These initial results indicate that LYVE-1 contributed to DC migration *via* dermal lymphatics.

Deficient DC entry to afferent dermal lymphatics in *Lyve1*$^{-/-}$ mice

LYVE-1 is expressed on both luminal and basolateral surfaces of lymph vessel endothelium[24]. To investigate whether the delay in DC trafficking between skin and draining inguinal or axial LNs in *Lyve1*$^{-/-}$ mice was due to a defect in initial lymphatic vessel entry or subsequent intraluminal migration, we visualized the transit of bone marrow-derived DCs (BMDCs) through the dermal lymphatics by confocal imaging. In oxazolone-sensitized *Lyve1*$^{-/-}$ and *Lyve1*$^{+/+}$ littermate mice injected with LPS-activated, CMFDA-labeled BMDMs, the cells were still visible in large numbers near the injection site 24 h post-injection **(Fig. 1c),** in agreement with reports that only approximately 1% of intradermally injected BMDCs reach draining LNs within this time-frame[4]. In *Lyve1*$^{+/+}$ BALB/c mice, CMFDA^{+} BMDCs were distributed along podoplanin stained dermal lymphatic vessels at 18 h and 24 h (**Fig. 1b, c**) and orthogonal views of z-stacks revealed that the majority of CMFDA^{+} cells associated with these lymphatics (85%) were inside the vessel lumen (**Fig. 1c, d**). In contrast, the distribution of CMFDA^{+} BMDCs in LYVE-1-deficient mice was largely independent of podoplanin^{+} lymphatics at 18 h (**Fig. 1b**), and those associated with podoplanin^{+} lymphatics accumulated at the basolateral surface of the vessels with only 22% present in the vessel lumen at 24 h, suggesting that their transit was stalled in the absence of LYVE-1 (**Fig. 1c, d**). Moreover, the number of dermally injected CMFDA^{+} BMDCs recovered in skin-draining LNs of oxazolone-sensitized Lyve1$^{-/-}$ mice (3 x 10^{3}) was 3-fold lower than in *Lyve1*$^{+/+}$ littermates (9 x 10^{3}, **Fig. 1e**), and total lymph node cellularity was 2.5-fold lower (1.9 x 10^{6} in *Lyve1*$^{-/-}$ mice compared with 8 x 10^{5} in *Lyve1*$^{+/+}$ littermates **Fig. 1f**). These results indicate that LYVE-1 contributed to the access of DCs to the vessel lumen.

Compromised egress of DCs from *Lyve1*$^{-/-}$ dermal explants

We next used short-term (24 h) *ex-vivo* crawl-out assays[25] to investigate DC trafficking in cultured skin explants from *Lyve1*$^{-/-}$ and *Lyve1*$^{+/+}$ BALB/c littermates. These assays measure the numbers of endogenous dermal DCs and epidermal Langerhans cells migrating from the skin through afferent dermal lymphatics into the culture medium, following mobilization by IL-18, IL-1β and TNF released within the excised tissue[26,27]. Freshly excised skin contained similar numbers of resident CD45^{+}MHCII^{+} leukocytes in *Lyve1*$^{-/-}$ and *Lyve1*$^{+/+}$ littermates **(Fig. 2a-b)**. However, following 24 h of *ex vivo* incubation, the number of CD45^{+}MHCII^{+} cells recovered in the medium from the *Lyve1*$^{-/-}$ explants (2 x 10^3) was 17-fold lower than in *Lyve1*$^{+/+}$ explants (3.4 x 10^4), **Fig. 2c-f**), comprising both CD103^{+} and CD11b^{+} DC populations. Overall these results indicate a role for LYVE-1 in the egress of dermal DCs from mouse skin explants.

DC trafficking involves interaction with LYVE-1 HA-binding domain

We next examined the consequences of blocking LYVE-1 function *in vivo* in *Lyve1*$^{+/+}$ BALB/c mice with a panel of blocking mAbs. We used 'house-made' rat anti-mouse LYVE-1 mAbs (B1/10 and C1/8)[28,29] and commercially available (mAb2125, R & D Systems) antibodies that bind epitopes within the Link domain of LYVE-1, which binds HA. All three mAbs bound both soluble LYVE-1 and LYVE-1-expressed on the surface of transfected Jurkat cells, and blocked binding of purified high molecular weight HA to LYVE-1 effectively, albeit with different affinities (mAb 2125 > B1/10 > C1/8) and relative potencies (IC_{50} mAb2125 < B1/10 < C1/8; **Supplementary Fig. 5a-c)**. Binding studies using LYVE-1 site-directed mutants and mapping onto a structure-based LYVE-1 model indicated that the C1/8 and mAb2125 epitopes are most similar to each other and bracket the predicted HA-binding cleft on the surface of LYVE-1, binding to residues Gln-50 and Asn136[30], while the epitope of

B1/10 appears to lie towards the opposite face, contacting residues Arg-98 and Phe-100 (**Supplementary Fig. 5d**).

The administration of saturating doses of either mAb2125 or C1/8 to oxazolone-sensitized *Lyve1*$^{+/+}$ BALB/c mice caused a 5-fold reduction in the number of endogenous, FITC-labeled (by skin painting), CD11c^{+} DCs recovered from the draining LNs at 24 h (**Fig. 3a**), along with a reduction in both the number of LN CD45^{+} cells and all subsets of CD11c^{+}MHCII^{+} DCs (**Supplementary Fig. 5e**) in comparison with *Lyve1*$^{+/+}$ mice receiving rat IgG. There was no significant reduction in the numbers of CD11c^{+} FITC-labeled DC recovered from the draining LNs of mice that were administered saturating doses of mAb B1/10 compared to rat IgG treated controls (**Supplementary Fig. 3a**), suggesting that the discrete epitope within the LYVE-1 HA-binding surface for this antibody is not involved in DC recruitment. Reduced accumulation of FITC^{+}CD11c^{+} DC in the draining LNs of C1/8- and mAb2125-treated mice was observed after 24h in both the sensitization and challenge phases of oxazolone hypersensitivity (**Fig. 3a, b**) and was equally effective in both BALB/c and C57BL/6 mice (**Fig. 3b, c**). Moreover, the inhibitory effects of C1/8 and mAb2125 on DC migration were sustained over 48 h post oxazolone-sensitization **(Fig. 3d)**, in marked contrast to the transient delay in DC recruitment seen in the *Lyve1*$^{-/-}$ mice. These results suggest that DC migration in dermal lymphatics is mediated by interactions between LYVE-1 and its ligand, HA.

We then used confocal microscopy to visualize lymphatic transit in oxazolone-sensitized BALB/c *Lyve1*$^{+/+}$ mice injected with the anti-LYVE-1 mAbs C1/8, B1/10 and mAb2125, 24 h after intradermal transfer of CMFDA-labeled BMDCs. C1/8 and mAb2125 injections caused an accumulation of these CMFDA labeled cells at the outer (basolateral) surface of the LYVE-1^{+} lymphatic capillaries compared to rat IgG controls, whereas B1/10 injection had no such effect (**Fig. 3e**).

Quantifying confocal images of skin sections indicated fewer than 20% of vessel-associated $CMFDA^+$ BMDCs were present within the lumen in C1/8- and mAb2125-treated mice, whereas > 80% of vessel-associated $CMFDA^+$ BMDCs were intraluminal in control IgG or B1/10-treated mice **(Fig. 3f)**. In addition, C1/8 and mAb2125 treatment elicited 5-fold reductions in the number of $CMFDA^+$ BMDCs recovered in the draining LNs of oxazolone-sensitized mice at 24 h after intradermal injection compared to rat IgG controls **(Fig. 3g)**.

We also investigated the effects of LYVE-1 mAb blockade on endogenous $CD45^+MHCII^+$ DC migration in dermal lymphatics of cultured BALB/c skin explants using the *ex vivo* crawl-out assay that quantifies the recovery of egressed cells in the surrounding media (supernatant) after 24 h. Treatment with C1/8 or mAb2125 over this period caused a significant 1.6-fold reduction in the numbers of $CD45^+MHCII^+$ cells collected from the explant supernatants compared to rat IgG treated controls, whereas B1/10 had no significant effect (**Fig. 3h**). This was mirrored by a reciprocal increase in $CD45^+MHCII^+$ DC numbers retained within the dermis in C1/8- and mAb2125-treated explants (**Fig. 3i**), indicating that targeting LYVE-1-HA-interaction prevents DC exit *via* dermal lymphatics. These results show that disruption of LYVE-1-HA interactions by LYVE-1 blocking mAbs impaired lymphatic trafficking of DCs at the point of initial vessel entry, and that similar interference reduced DC egress from dermal tissue explants.

***LYVE-1*-mediated DC migration promotes LN CD8 T-cell responses**

Next, we examined the physiological importance of LYVE-1-mediated DC trafficking for antigen delivery and cell-mediated immune responses in draining LNs. We measured the effects of LYVE-1 C1/8 and B1/10 mAb administration on the F5 transgenic $CD8^+$ T-cell response to influenza virus A/NT/60/68 nucleoprotein (NP) peptide ASNENDAM[28,31] expressed from a modified vaccinia virus Ankara (MVA)-

vectored MVA.HIVA.NP vaccine in C57BL/10 mice. Mice adoptively transferred (i.v.) with CFSE-labeled F5 T-cells were injected (i.p.) with LYVE-1 mAbs 24 h before and after intradermal MVA.HIVA.NP vaccination. In this model, peptide is delivered to LNs through virus uptake by migrating dermal APCs [28] and hence depends on efficient migration of antigen-loaded DCs through afferent lymphatic capillaries. Administration of mAb C1/8 reduced the number of proliferating NP-specific F5 $CD8^+$ T-cells in the draining cervical LNs by more than 40% compared to rat IgG treated controls, as determined by CFSE dilution 72h post-challenge, whereas the LYVE-1 mAb B1/10, which failed to block DC trafficking to skin-draining LNs had no appreciable effect (**Fig. 4a, b).** Importantly, i.p. injection of C1/8 did not alter proliferation of F5 T-cells in the spleens of mice immunized intravenously with MVA.HIVA.NP compared to rat IgG injected controls **(Fig 4c)**. Because the spleen lacks an afferent lymphatic supply, these results indicated that the LYVE-1-HA blocking mAbs specifically targeted afferent lymphatic trafficking.

We also investigated the proliferative response of adoptively transferred (i.v.) CFSE-labeled ovalbumin-specific OT1 $CD8^+$ T-cells in the draining LNs of *Lyve1*$^{-/-}$ C57BL/6 and control *Lyve1*$^{+/+}$ littermate recipients after intradermal transfer of BMDCs pulsed with ovalbumin peptide *ex vivo*. We observed a 25% reduction in numbers of proliferating OT-1 $CD8^+$ T-cells in the draining cervical nodes of LYVE-1-deficient mice (44.8%) than in *Lyve1*$^{+/+}$ littermates (59.7%) as determined by CFSE labeling 44 h after transfer of antigen-loaded DCs **(Fig. 4d, e)**. Furthermore, OT-1 $CD8^+$ T-cells transferred into Lyve1$^{-/-}$ mice exhibited lower expression of the T-cell activation markers CD25 and CD69 compared to *Lyve1*$^{+/+}$ littermate controls (**Fig. 4f** and data not shown). We could not detect T-cell proliferation or upregulation of activation markers in non-draining LNs (data not shown). These results indicate that

interference with LYVE-1 blocks lymph node T-cell proliferation to dermally administered peptide antigens.

LYVE-1 engages migrating DCs via their endogenous surface HA

To investigate whether DC entry to lymphatics is modulated by LYVE-1 interaction with HA on the DC surface[32,33], we first incubated BMDCs with recombinant biotin-labeled versican G1 domain (bVG1), a high-affinity HA-binding protein reagent used to detect HA on the surface of cells[34,35]. bVG1 stained approximately 50% of $CD11c^{+}MHCII^{+}$ BMDCs, as assessed by confocal microscopy and flow cytometry (**Fig. 5a-b** and **Supplementary Fig. 4b**). Using a sensitive competitive ELISA, we also detected HA in whole cell lysates and supernatants of both immature and LPS-activated BMDCs (**Fig. 5c-d**). Additionally, as assessed by RT-PCR, BMDCs expressed *HAS2* mRNA, encoding the key hyaluronan synthase protein[32] (**Fig. 5e**), suggesting a capacity for endogenous HA synthesis. HA was also detected on human monocyte-derived DCs (MDDCs) (**Fig. 5f-g**), and expression increased upon LPS-induced maturation (**Fig. 5h**).

To assess whether HA was expressed by tissue-resident DC populations *in vivo*, we stained ear skin from *Lyve1*$^{+/+}$ mice with bVG1, both *in situ* in whole-mount tissue sections and *ex vivo*, in cytospin preparations of dermal DCs egressed from *ex vivo* cultured dermal explants collected after 24 h. Because CD11c mAbs failed in whole-mount staining protocols we used immunostaining with MHCII antibody and bVG1 in transgenic CD11c-GFP fluorescent DC reporter mice to identify endogenous $CD11c^{+}$ DC (**Supplementary Fig. 6**). HA expression was detected on a large proportion (67%) of resident CD11c-$GFP^{+}MHCII^{+}$ DCs *in situ* in skin sections of these mice **(Fig 5i),** but on all CD11c-$GFP^{+}MHCII^{+}$ DCs that had egressed after 24 h from the cultured dermal explants **(Fig. 5j)** indicating an enrichment of the glycosaminoglycan in this latter population.

To directly test if HA is required for DC migration through lymphatic vessels, we depleted HA from the surface of immature BMDCs by digestion with purified hyaluronidase (HAase), followed by 72 h treatment in culture with 4-methylumbelliferone (4-MU), a non-toxic HA synthase inhibitor, to prevent replenishment by *de novo* re-synthesis during subsequent LPS-induced DC maturation. Such treatment decreased HA levels to approximately 50% of those in mock-treated BMDCs and these remained stable 24 h after removal of 4-MU (**Fig. 6a, b**), but did not significantly affect BMDC viability, surface integrin integrity or expression of CD86 used as a measure of activation (**Supplementary Fig. 4c-e**). To assess the effects on lymphatic migration, HAase/4-MU- and mock-treated BMDCs, tagged with Q-dot® 585 or Q-dot® 655, respectively were co-injected intradermally into oxazolone-sensitized BALB/c *Lyve1*$^{+/+}$ mice, followed by flow cytometry to assess the numbers of labeled BMDC in the draining LNs. 24 h post-transfer we recovered up to 3-fold more mock-treated DCs than HAase/4-MU-treated DCs from the draining LNs, with the latter exhibiting diminished surface expression of HA at this time point **(Fig. 6c, h)**. These data indicate that DCs express HA on their surface both *in vitro* and *in vivo*, and suggest that HA expression is important for trafficking *via* afferent lymphatics.

LYVE-1-HA interactions mediate DC adhesion and transmigration

To define the molecular mechanisms by which LYVE-1 and HA mediate DC trafficking through lymphatics, we used *in vitro* adhesion and transendothelial migration assays in which CMFDA-labeled, LPS-matured BMDCs were co-incubated over monolayers of primary LYVE-1^{+} mouse dermal LECs (mLECs) isolated from BALB/c neonatal skin using immunomagnetic bead selection with LYVE-1 mAb C1/8[15] and plated on plastic multiwell dishes or on the undersurface of light-opaque transwell inserts respectively. Co-incubation (2 h) with either mAb2125 or C1/8

reduced the number of BMDCs adhering to the mLEC monolayers by 2-fold compared to isotype-matched control rat IgG, whereas B1/10 had no significant effect (**Fig. 7a).** Likewise, pre-incubation (2h) with purified hyaluronidase reduced the number of BMDCs adhering to mLEC monolayers by more than 3-fold compared to mock treated controls, whereas hyaluronidase treatment of mLECs had no such effect (**Fig. 7b**), indicating that HA expressed by BMDCs is required for the interaction. Moreover, inclusion of C1/8 or mAb2125 throughout the duration (12h) of transwell assay cultures reduced BMDC basolateral-to-luminal transmigration through the mLEC layer by 2-fold in each case, as assessed by quantitation of fluorescent (CMFDA) cell numbers, compared to a rat IgG isotype control, while B1/10 showed no statistically significant effect (**Fig. 7c-e**). These results indicate both DC adhesion and migration across a LEC monolayer involved LYVE-1 interaction with HA on the DC surface.

Docking to lymphatic endothelium via LYVE-1 transmigratory cups

We next used high-magnification confocal microscopy of BMDCs co-cultured with primary mLEC monolayers to image the DC:LEC interface and visualize how the interaction between HA and LYVE-1 facilitates adhesion and transmigration. We observed that adherent BMDCs docked to the mLEC monolayer surface in discrete ring-like structures that stained intensely for LYVE-1 (**Fig. 7f**). In z-stack orthogonal views of the confocal images the ring-like structures appeared as cups that extended from the endothelium, partly enveloping the adherent DCs (**Fig. 7g, h**). Addition of C1/8 or mAb2125 to the mLEC-BMDC co-cultures, or HAase pre-treatment of the BMDCs greatly reduced the number of LYVE-1^+ cups that formed on the mLEC monolayer surface compared to a rat IgG isotype control (**Fig. 8a-b and Supplementary Fig. 7**), implying that the interaction between LYVE-1 and HA on the surface of BMDC contributed to the stability of these molecular structures.

Similar LYVE-1$^+$ cups were observed on primary human LEC (hLEC) monolayers incubated with human MDDCs (Supplementary Fig. 7) and their formation was inhibited by the addition of the human LYVE-1-HA blocking mAb 891 (**Fig. 8c** and **Supplementary Fig. 7**). In addition, in frozen skin sections from oxazolone-sensitized BALB/c mice, HA was closely associated with endogenous MHCII$^+$ DCs that were undergoing transmigration into lymphatic vessels (**Fig. 8d**). Finally, in skin sections from oxazolone-sensitized mice injected intradermally with CMFDA-labeled BMDCs, these were observed in close contact with LYVE-1$^+$ protrusions of lymphatic vessels during diapedesis (**Fig. 8e** and **Supplementary Fig. 8**). These results show that adhesion of DC to LECs involved formation of LYVE-1+ endothelial "transmigratory cups" through interaction with DC HA, and provide evidence they form both *in vitro* and *in vivo*.

Discussion

Here we have revealed that the endothelial HA receptor LYVE-1 is an important mediator of leukocyte trafficking. LYVE-1 promoted the docking of DCs to lymphatic vessel endothelium within dynamic endothelial transmigratory cups, by engaging HA expressed by DC[32]. Using a topical oxazolone-induced model of skin hypersensitivity in mice, *ex vivo* dermal crawl-out assays, *in vitro* transmigration assays and fluorescent imaging we showed that genetic deletion of *Lyve1* or functional disruption by mAbs that interfere with HA-LYVE-1 interactions impaired early transit of DCs through dermal lymphatic capillaries to draining LNs, by preventing their interaction with the lymphatic endothelium. Endothelial cup formation, adhesion and transmigration and LN trafficking were all impaired by enzymatic removal of HA on the surface of DC and prolonged inhibition of endogenous HA biosynthesis. Lastly, *Lyve1* gene deletion or antibody blockade

significantly reduced the $CD8^+$ T-cell responses to peptide antigens in the lymph nodes. As such, LYVE-1-HA interaction mediated a rate-limiting step for DC lymphatic entry and the initiation of immune responses in skin draining lymph nodes.

The transient nature of the DC trafficking defect in *Lyve1*$^{-/-}$ mice and the more sustained effects of LYVE-1 antibody blockade in adult *Lyve1*$^{+/+}$ mice, suggest compensatory mechanisms during embryonic development in mice with genomic deletion of *Lyve1*, a phenomenon previously suggested for mice deficient in the primary leukocyte HA receptor CD44[36,37]. Compensation through functional redundancy may account for the apparently normal phenotype of *Lyve1*$^{-/-}$ mice under normal homeostatic conditions. Moreover, the comparatively short duration of the trafficking defects in the *Lyve1*$^{-/-}$ mice, particularly those on the C57BL/6 background, provides an explanation for the failure to identify an important trafficking role for LYVE-1 in earlier, more limited studies[23]. Clearly, more detailed studies of lymphatic trafficking in mice using live imaging and conditional or acute deletion of *Lyve1* will be required to fully define such phenomena in the future.

A function for LYVE-1 as a lymph-specific trafficking receptor is fully consistent with its segregated expression at the tips of the interdigitating endothelial junctions of initial lymphatic vessels, which act as hotspots for DC entry *in vivo*[13]. HA-mediated docking with LYVE-1 at these sites could facilitate DC transmigration not only through direct adhesion, but also through the local unbuttoning of endothelial junctions. In support of this view, it is documented that LYVE-1 can transduce signals for VE-cadherin turnover and endothelial junctional remodeling in LEC-like cell lines *in vitro*[38], a process triggered by LYVE-1 mAbs and HA-binding in primary LEC (Wang *et al*, manuscript in preparation). Although the LEC monolayers used here do not spontaneously assemble interdigitating button-like junctions during *in vitro* culture but instead form continuous zipper-like junctions, these are plastic *in vivo* and

can transition between the two states according to tissue inflammatory status[39]. Hence, the LYVE-1$^+$ transmigratory cups we observed in mouse and human LECs likely reflect authentic physiological structures. The analogous LYVE-1$^+$ membranous protrusions we observed around dermal DCs undergoing vessel entry in mouse skin lends further credence to this notion.

The role played by LYVE-1 in lymphatic trafficking bears comparison with the closely related leukocyte HA receptor CD44, which mediates lymphocyte and neutrophil capture from laminar blood flow by engaging HA from the luminal glycocalyx in inflamed vascular endothelium[40]. Importantly, the avidity of the CD44:HA interaction necessary for such capture depends on the capacity of HA to form prior crosslinked complexes with inflammation-associated binding partners such as TSG-6[41], or adduct formation with serum-derived HA associated protein (SHAP) [21,42,43]. In lymphatic vessels, LYVE-1 must instead play a reciprocal role by engaging HA arrayed on the leukocyte surface. Although we have yet to determine whether DCs organize this surface HA within similar crosslinked complexes, it is noteworthy that they can synthesize both TSG-6 and the heavy chain of inter alpha trypsin inhibitor (IαI) that generates SHAP[44,45]. Moreover, native LYVE-1 has a marked preference for binding crosslinked HA-TSG-6 complexes, which harness avidity by inducing receptor surface clustering[46]. This preference is exploited by pathogenic Group A hemolytic streptococci to bind LYVE-1 through their dense HA surface capsule for enhanced dissemination to host LNs[47]. Hence the properties of LYVE-1 appear ideally suited for selective docking with cell surface HA assemblages rather than free ambient HA in the tissue matrix. Indeed, LYVE-1-HA bonds form more rapidly and rupture more easily than CD44-HA bonds in response to force, despite their similar binding affinities (K_d 8-100 μM) (Bano, F., Banerji, S. Jackson, D.G. and Richter,R.R. unpublished), in keeping with a role in supporting DC crawling at the

lymphatic vessel surface, where lower shear forces are encountered in comparison with those in venous blood flow[48].

Finally, while our current study highlighted the role of LYVE-1 in mediating DC entry to dermal lymphatic vessels, it is possible that the receptor also facilitates trafficking in LNs, where its location in the subcapsular sinus floor would suggest a role in movement of DCs from lymph to the T-cell-rich paracortex. Both in the subcapsular sinus floor and in peripheral lymphatics, LYVE-1 likely mediates migration of a variety of immunomodulatory populations besides DCs. Notably, monocytes and macrophages also synthesize HA, and human monocyte-derived macrophages employ LYVE-1 and HA for transmigration across LECs *in vitro*[46]. In contrast, neutrophils, which exit skin *via* lymph in response to bacterial infection appear not to utilize LYVE-1 for vessel entry, but rather an unusual β2 integrin- and lipoxin-mediated mechanism[49,50]. The degree of LYVE-1 involvement may well depend on the nature and extent of leukocyte HA organization and the particular choice of vessel sites these cells target for entry.

In conclusion, we have shown that the LYVE-1-HA interaction constitutes a physiologically important axis regulating DC trafficking in lymph. Consequently, LYVE-1 has the potential as a therapeutic target for limiting inflammation and associated immune activation.

Data availability

The data that support the findings of this study are available from the corresponding author upon request**.**

Acknowledgments

This work was supported by the UK Medical Research Council through MRC Human Immunology Unit core funding and Project Grant MR/L008610/1 to D.G.J. The

authors would also like to acknowledge the now deceased M. Puklavec (Sir William Dunn School of Pathology, Oxford), for his invaluable technical advice on making rat monoclonal antibodies, and the Wolfson Imaging Centre, Weatherall Institute of Molecular Medicine, Oxford for use of the fluorescence microscope equipment in this project. The authors also thank P. Sopp, C. Waugh, K. Clark and S.-A. Clark from the WIMM Flow Cytometry Facility, for their excellent technical assistance and advice.

Author Contributions

L.A.J. and D.G.J. designed experiments, interpreted the data and wrote the manuscript, S.B. performed experiments, helped interpret the data and edited the manuscript. L.A.J., U.G. and G.P. performed experiments and analyzed data, W.L., K.A.H., and Y.M.R. performed experiments and provided reagents, T.H., V.C. and N.W.G. provided critical reagents and helped edit the manuscript.

Competing Financial Interests

The authors declare no competing financial interests.

References

1. Mellman, I. & Steinman, R. M. Dendritic cells: specialized and regulated antigen processing machines. *Cell* **106,** 255–258 (2001).
2. Randolph, G. J., Ivanov, S., Zinselmeyer, B. H. & Scallan, J. P. The Lymphatic System: Integral Roles in Immunity. *Annu. Rev. Immunol.* **35,** annurev-immunol-041015-055354 (2017).
3. Miteva, D. O. *et al.* Transmural flow modulates cell and fluid transport functions of lymphatic endothelium. *Circ Res* **106,** 920–931 (2010).
4. Martín-Fontecha, A. *et al.* Regulation of dendritic cell migration to the draining lymph node: impact on T lymphocyte traffic and priming. *J Exp Med* **198,** 615–621 (2003).
5. Lammermann, T. *et al.* Rapid leukocyte migration by integrin-independent flowing and squeezing. *Nature* **453,** 51–55 (2008).
6. Johnson, L. A. & Jackson, D. G. Inflammation-induced secretion of CCL21 in lymphatic endothelium is a key regulator of integrin-mediated dendritic cell transmigration. *Int Immunol* **22,** 839–849 (2010).
7. Johnson, L. A. & Jackson, D. G. The chemokine CX3CL1 promotes trafficking of dendritic cells through inflamed lymphatics. *J Cell Sci* **126,** 5259–5270 (2013).
8. Kabashima, K. *et al.* CXCL12-CXCR4 engagement is required for migration of cutaneous dendritic cells. *Am J Pathol* **171,** 1249–1257 (2007).
9. Teijeira, A., Russo, E. & Halin, C. Taking the lymphatic route: dendritic cell migration to draining lymph nodes. *Semin Immunopathol* (2014). doi:10.1007/s00281-013-0410-8
10. Russo, E. *et al.* Intralymphatic CCL21 Promotes Tissue Egress of Dendritic Cells through Afferent Lymphatic Vessels. *Cell Rep.* **14,** 1723–1734 (2016).

11. Weber, M. *et al.* Interstitial dendritic cell guidance by haptotactic chemokine gradients. *Science (80-.).* **339,** 328–332 (2013).

12. Takamatsu, H. *et al.* Semaphorins guide the entry of dendritic cells into the lymphatics by activating myosin II. *Nat Immunol* **11,** 594–600 (2010).

13. Baluk, P. *et al.* Functionally specialized junctions between endothelial cells of lymphatic vessels. *J Exp Med* **204,** 2349–2362 (2007).

14. Pflicke, H. & Sixt, M. Preformed portals facilitate dendritic cell entry into afferent lymphatic vessels. *J Exp Med* **206,** 2925–2935 (2009).

15. Johnson, L. A. *et al.* An inflammation-induced mechanism for leukocyte transmigration across lymphatic vessel endothelium. *J Exp Med* **203,** 2763–2777 (2006).

16. Nitschke, M. *et al.* Differential requirement for ROCK in dendritic cell migration within lymphatic capillaries in steady-state and inflammation. *Blood* **120,** 2249–2258 (2012).

17. Teijeira, A. *et al.* Lymphatic Endothelium Forms Integrin-Engaging 3D Structures during DC Transit across Inflamed Lymphatic Vessels. *J Invest Dermatol* **133,** 2276–2285 (2013).

18. Irjala, H. *et al.* Mannose receptor is a novel ligand for L-selectin and mediates lymphocyte binding to lymphatic endothelium. *J Exp Med* **194,** 1033–1041 (2001).

19. Salmi, M., Koskinen, K., Henttinen, T., Elima, K. & Jalkanen, S. CLEVER-1 mediates lymphocyte transmigration through vascular and lymphatic endothelium. *Blood* **104,** 3849–3857 (2004).

20. Banerji, S. *et al.* LYVE-1, a new homologue of the CD44 glycoprotein, is a lymph-specific receptor for hyaluronan. *J. Cell Biol.* **144,** 789–801 (1999).

21. McDonald, B. & Kubes, P. Interactions between CD44 and Hyaluronan in

Leukocyte Trafficking. *Front Immunol* **6,** 68 (2015).

22. Cumberbatch, M., Dearman, R. J., Griffiths, C. E. & Kimber, I. Epidermal Langerhans cell migration and sensitisation to chemical allergens. *Apmis* **111,** 797–804 (2003).

23. Gale, N. W. *et al.* Normal lymphatic development and function in mice deficient for the lymphatic hyaluronan receptor LYVE-1. *Mol Cell Biol* (2006).

24. Prevo, R., Banerji, S., Ferguson, D. J. P., Clasper, S. & Jackson, D. G. Mouse LYVE-1 is an endocytic receptor for hyaluronan in lymphatic endothelium. *J. Biol. Chem.* **276,** 19420–19430 (2001).

25. Stoitzner, P., Romani, N., McLellan, A. & Tripp, C. Isolation of skin dendritic cells from mouse and man. *Methods Mol.* … (2010).

26. Larsen, C. P. *et al.* Migration and maturation of Langerhans cells in skin transplants and explants. *J Exp Med* **172,** 1483–1493 (1990).

27. Cumberbatch, M., Dearman, R. J., Antonopoulos, C., Groves, R. W. & Kimber, I. Interleukin (IL)-18 induces Langerhans cell migration by a tumour necrosis factor-alpha- and IL-1beta-dependent mechanism. *Immunology* **102,** 323–330 (2001).

28. Teoh, D., Johnson, L. A., Hanke, T., McMichael, A. J. & Jackson, D. G. Blocking development of a CD8+ T-cell response by targeting lymphatic recruitment of antigen presenting cells. *J. Immunol.* **182,** (2009).

29. Johnson, L. A., Prevo, R., Clasper, S. & Jackson, D. G. Inflammation-induced uptake and degradation of the lymphatic endothelial hyaluronan receptor LYVE-1. *J Biol Chem* **282,** 33671–33680 (2007).

30. Banerji, S., Hide, B. R., James, J. R., Noble, M. E. & Jackson, D. G. Distinctive properties of the hyaluronan-binding domain in the lymphatic endothelial receptor Lyve-1 and their implications for receptor function. *J Biol*

Chem **285,** 10724–10735 (2010).

31. Estcourt, M. J., McMichael, A. J. & Hanke, T. Altered primary CD8+ T-cell response to a modified virus Ankara(MVA)-vectored vaccine in the absence of CD4+ T-cell help. *Eur J Immunol* **35,** 3460–3467 (2005).

32. Mummert, M. E. *et al.* Synthesis and surface expression of hyaluronan by dendritic cells and its potential role in antigen presentation. *J Immunol* **169,** 4322–4331 (2002).

33. Chang, M. Y. *et al.* A rapid increase in macrophage-derived versican and hyaluronan in infectious lung disease. *Matrix Biol* **34,** 1–12 (2014).

34. de la Motte, C. A. & Drazba, J. A. Viewing hyaluronan: imaging contributes to imagining new roles for this amazing matrix polymer. *J Histochem Cytochem* **59,** 252–257 (2011).

35. Clark, S. J. *et al.* Mapping the differential distribution of glycosaminoglycans in the adult human retina, choroid, and sclera. *Invest Ophthalmol Vis Sci* **52,** 6511–6521 (2011).

36. Schmits, R. *et al.* CD44 regulates hematopoietic progenitor distribution, granuloma formation, and tumorigenicity. *Blood* **90,** 2217–2233 (1997).

37. Protin, U., Schweighoffer, T., Jochum, W. & Hilberg, F. CD44-deficient mice develop normally with changes in subpopulations and recirculation of lymphocyte subsets. *J. Immunlogy* **163,** 4917–4923 (1999).

38. Hou, W. H. *et al.* CRSBP-1/LYVE-1 ligands disrupt lymphatic intercellular adhesion by inducing tyrosine phosphorylation and internalization of VE-cadherin. *J Cell Sci* **124,** 1231–1244 (2011).

39. Yao, L. C., Baluk, P., Srinivasan, R. S., Oliver, G. & McDonald, D. M. Plasticity of button-like junctions in the endothelium of airway lymphatics in development and inflammation. *Am J Pathol* **180,** 2561–2575 (2012).

40. Siegelman, M. H., DeGrendele, H. C. & Estess, P. Activation and interaction of CD44 and hyaluronan in immunological systems. *J. Leukoc. Biol.* **66,** 315–21 (1999).

41. Lesley, J. *et al.* TSG-6 modulates the interaction between hyaluronan and cell surface CD44. *J. Biol. Chem.* **279,** 25745–25754 (2004).

42. de la Motte, C. a, Hascall, V. C., Drazba, J., Bandyopadhyay, S. K. & Strong, S. a. Mononuclear leukocytes bind to specific hyaluronan structures on colon mucosal smooth muscle cells treated with polyinosinic acid:polycytidylic acid: inter-alpha-trypsin inhibitor is crucial to structure and function. *Am. J. Pathol.* **163,** 121–133 (2003).

43. Petrey, A. C. & de la Motte, C. A. Hyaluronan, a crucial regulator of inflammation. *Front Immunol* **5,** 101 (2014).

44. Maina, V. *et al.* Coregulation in human leukocytes of the long pentraxin PTX3 and TSG-6. *J. Leukoc. Biol.* **86,** 123–132 (2009).

45. Chang, M. Y. *et al.* Monocyte-to-macrophage differentiation: Synthesis and secretion of a complex extracellular matrix. *J. Biol. Chem.* **287,** 14122–14135 (2012).

46. Lawrance, W., Banerji, S., Day, A. J., Bhattacharjee, S. & Jackson, D. G. Binding of hyaluronan to the native lymphatic vessel endothelial receptor LYVE-1 is critically dependent on receptor surface clustering and hyaluronan organisation. *J Biol Chem* (2016). doi:10.1074/jbc.M115.708305

47. Lynskey, N. N. *et al.* Rapid Lymphatic Dissemination of Encapsulated Group A Streptococci via Lymphatic Vessel Endothelial Receptor-1 Interaction. *PLoS Pathog* **11,** e1005137 (2015).

48. Bano, F., Banerji, S., Howarth, M., Jackson, D. G. & Richter, R. P. A single molecule assay to probe monovalent and multivalent bonds between

565 hyaluronan and its key leukocyte receptor CD44 under force. *Sci Rep* **6,** (2016).
566 49. Hampton, H. R., Bailey, J., Tomura, M., Brink, R. & Chtanova, T. Microbe-
567 dependent lymphatic migration of neutrophils modulates lymphocyte
568 proliferation in lymph nodes. *Nat Commun* **6,** 7139 (2015).
569 50. Rigby, D. A., Ferguson, D. J., Johnson, L. A. & Jackson, D. G. Neutrophils
570 rapidly transit inflamed lymphatic vessel endothelium via integrin-dependent
571 proteolysis and lipoxin-induced junctional retraction. *J Leukoc Biol* **98,** 897–
572 912 (2015).
573
574

575 **Figure legends**

576

577 **Fig. 1. Impaired entry of DCs to dermal lymphatic vessels in BALB/c *Lyve1*$^{-/-}$**
578 **mice. (a)** Recovery of endogenous DCs from draining inguinal and axillary LNs at
579 indicated time intervals after topical application of oxazolone and FITC, as measured
580 by flow cytometry. Data represent the mean ± s.e. (n = 5), from one experiment of
581 three, with representative dot plots shown. **(b-c)** Entry of CMFDA-labeled BMDCs
582 (green) into podoplanin^{+} (red) afferent lymphatics of *Lyve1*$^{-/-}$ and *Lyve*$^{-+/+}$ litter mates,
583 as observed by confocal microscopy of whole mount sections of ear dermis, either 18
584 h (**b**) or 24 h (**c**) after topical application of oxazolone and intradermal injection of
585 BMDCs. Representative images from three separate repeated experiments are shown,
586 bar = 100μm. **(c)** Images of three-dimensional rendering of z-stacks are shown at low
587 magnification (250X, left panels), higher magnification (630X, middle panels) and
588 include orthogonal sections (right panels). (**d**) Numbers of BMDCs inside the lumens
589 of lymphatic vessels, expressed as a percentage of the number of lymphatic vessel-
590 associated BMDCs. Data are the mean values ± s.e. (n = 5 mice), from one
591 experiment of three. **(e, f)** Recovery of i.d. injected BMDCs (**e**) and overall cellularity
592 (**f**) in draining cervical LNs, 24 h after topical application of oxazolone and adoptive
593 transfer of BMDCs, as measured by flow cytometry. Data represent the mean ± s.e. (n
594 = 5), from one experiment of two. * $P < 0.05$; ** $P < 0.01$.

595 **Figure 2. Impaired egress of dermal DCs from *ex vivo* cultured split ear tissue of**
596 **BALB/c *Lyve1*$^{-/-}$ mice.** (**a-d**) Flow cytometric analysis of digested ear tissue from
597 wild-type *Lyve1*$^{-/-}$ mice and *Lyve*$^{+/+}$ littermates, either freshly resected (**a, b**) or
598 following *ex vivo* culturing for 24 h (**c, d**). (**e, f**) Cells that had egressed from the
599 dermis into the tissue culture medium were also analyzed by flow cytometry. Data

shown by representative dot plots (**a, c, e**) and bar-and-whiskers bar charts (**b, d, f**), mean ± s.e. (n= 5) from one experiment of three, **P < 0.01.

Figure 3. Anti-LYVE-1-specific mAbs inhibit *in vivo* trafficking of DCs through dermal lymphatics. (**a-b**) Recovery of endogenous DCs in draining LNs, in BALB/c mice following injections of rat IgG or anti-LYVE-1 mAbs B1/10, C1/8 or mAb2125, during either sensitization (**a**) or challenge (**b**) of oxazolone/FITC painting. Data show numbers of $CD45^+FITC^+CD11c^+$ DCs, (n = 5), one experiment of three. (**c**) Effect of anti-LYVE-1 mAbs on DC trafficking in C57BL/6 mice, 24 h following oxazolone/FITC painting, with anti-ICAM-1 mAb YN1-1 as a positive control, (n = 4), one experiment of three. **(d)** Recovery of DCs in draining LNs, 6-48 h after oxazolone/FITC painting in BALB/c mice injected with rat IgG2a or C1/8, (n = 4), one experiment of two. (**e-f**) Entry of CMFDA-labeled BMDCs (green) into dermal afferent lymphatics immunostained with rabbit anti-LYVE-1 (blue) following oxazolone painting, magnification: 630X, bar = 20μm (Rat IgG and B1/10), bar = 50μm (C1/8 and mAb2125) **(e)**, expressed as a percentage of lymphatic vessel-associated BMDCs (**f**), (n = 5), one experiment of three, with representative images. Arrows indicate BMDCs within lymphatic vessel lumens; arrow-heads indicate BMDCs restricted to basolateral surfaces of vessels. (**g**) Recovery of BMDCs from draining LNs, 24 h after injection. (**h, i**) *Ex-vivo* skin crawl-out assays from ear tissue, showing numbers of egressed DCs (**h**) and remaining dermal DCs **(i)**, (n= 5), one experiment of three. Data expressed as the mean ± s.e. *n.s*., not significant; *P < 0.05; **P < 0.01.

Figure 4. Disruption of LYVE-1-mediated DC trafficking inhibits primary antigen-specific T-cell responses in skin-draining LNs. (**a,b**) Influenza NP-specific LN $CD8^+$ T-cell proliferation, in response to dermally injected MVA.HIVA.NP vaccine in C57BL/10 mice adoptively transferred with F5 transgenic T-cells and

injected with LYVE-1 mAbs, as determined by flow cytometry. Data are plotted as percentage of dividing F5 tetramer-reactive $CD8^+$ T-cells **(a)** with representative histograms of CFSE fluorescence, indicating levels of LN T-cell activation **(b)**. (**c**) Controls showing unaltered spleen $CD8^+$ F5 T-cell responses in mice injected i.v with MVA.HIVA.NP and the indicated LYVE-1 mAbs, as determined by flow cytometry, Data are the mean values ± s.e. (n = 3) from one experiment of three. *n.s.*, not significant; *P < 0.05. **(d,e)** Ovalbumin-specific LN $CD8^+$ T-cell responses elicited by peptide (SIINFEKL)-pulsed BMDCs after injection into C57BL/6 *Lyve1*$^{-/-}$ or wild-type *Lyve1*$^{+/+}$ mice, adoptively transferred with OT-1 transgenic T-cells. (**d**) Resulting LN T-cell proliferation status determined by flow cytometry, plotted as percentage of dividing OT-1 tetramer-reactive $CD8^+$ T-cells (**e**) and representative histograms of CFSE fluorescence and CD25 expression levels within gated cell populations shown, indicating levels of LN T-cell activation. No $CD8^+$ T-cell proliferation was detected in non-draining LNs. Data are the mean values ± s.e. (n = 8) from one experiment of two, analyzed by Student's T-test. ***P < 0.005.

Figure 5. DCs express HA as a cell surface coat. (**a-e**) Detection of HA in CMFDA-labeled BMDC (green), using biotinylated VG1 (bVG1) (red) following incubation in absence (mock) or presence of hyaluronidase (HAase), shown by confocal microscopy (**a**) and flow cytometry (**b**), with hyaluronidase-treated control cells (grey) and mock-treated cells (blue). Presence of HA in both BMDC lysates (**c**) and supernatants (**d**), both immature and following LPS-induced maturation, measured by ELISA, (n = 15). Expression of HAS mRNA in mature DCs shown by RT-PCR (**e**). (**f-g**) HA on mature human CMFDA-labeled MDDCs (green) using bVG1 (red), ± hyaluronidase, (**f**) and by flow cytometry, with hyaluronidase-treated control cells (grey) and mock-treated cells (blue), (**g**), with surface HA levels increasing following LPS-induced maturation (**h**), n = 5 from one representative experiment of three. (**i**)

Imaging of surface HA in endogenous dermal DCs in CD11cGFP (green) reporter mice, detected by bVG1 (blue) and immunostained with anti-MHCclII (red), ± hyaluronidase. (**j**) *Ex vivo* skin crawl-out assays showing percentage of $CD11cGFP^+$ $MHCclII^+$ DCs retained and egressed after 24h in culture, scored as surface HA^+ by microscopy, 4 mice per condition, from which three fields of view were assessed (n = 12), one experiment of three. Representative images from three separate repeated experiments are shown. Data represent the mean ± s.e., *P < 0.05; ***P < 0.005; ****P < 0.0001. Bar = 10μm.

Figure 6. HA is required for efficient lymphatic migration of DCs to skin-draining LNs. (a, b) Depletion of surface HA from mature BMDCs by hyaluronidase digestion and *in vitro* culture (72h) with 4-MU as assessed by streptavidin/bVG1 binding and flow cytometry. Graphs show surface HA levels on immature and mature bmDC incubated either alone (mock) or in the presence of 4-MU (**a**) and 24h after removal of 4-MU inhibition (**b**). Data are the mean ± s.e. (BMDCs from n = 4 mice), ****P < 0.0001, from one experiment of three. (**c-d)** Trafficking of control mock-treated and hyaluronidase/4-MU-treated BMDCs to draining LNs quantitated by differential labelling with Q-dot655 and Q-dot585 respectively (**c**, upper panels) or the reverse (lower panels), 24 h after 1:1 co-injection into the dermis of oxazolone-treated mice. Relative numbers of each BMDC population recovered in draining LNs are shown as dot plots and matched pair graphs (n = 5) with statistical analysis by paired Student's t-test, with representative FACS histograms for surface HA levels in Q-dot-labeled hyaluronidase/4-MU treated BMDCs (blue) recovered from cervical nodes compared to mock treated controls (grey). (**d**) Surface HA levels graphed as the mean ± s.e. (pooled from samples shown in **c**). Data are shown from one representative experiment of three. *P < 0.05; **P < 0.01.

Figure 7. DCs adhere to LECs in an HA- and LYVE-1-dependent manner *via* LYVE-1-enriched transmigratory cups. (**a-b**) Adhesion of LPS-matured, CMFDA-labeled BMDCs to primary mLEC monolayers after 3 h incubation in the presence of either irrelevant rat IgG or anti-LYVE-1 mAbs B1/10, C1/8 or mAb2125 (**a**) or following 2 h pre-incubation with hyaluronidase (HAase), (**b**), as assessed by fluorescence plate reader. (**c-e**) Basolateral-to-luminal transmigration of LPS-matured, fluorescently labeled BMDCs across mLEC monolayers grown on the undersurface of transwell filters quantitated over time by fluorescence plate reader in the presence of irrelevant rat IgG or anti-LYVE-1 mAbs B1/10 (**c**), C1/8 (**d**) or mAb2125 (**e**). Data are the mean ± s.e., one representative experiment of three, n = 4. *P < 0.05. (**f-h**) Confocal microscopy of cultured primary mLEC monolayers immunostained with rabbit anti-LYVE-1 (red), viewed 3 h after addition of fluorescently labeled BMDCs (green, CMFDA) and counter-stained with DAPI (grey, **g-h**). LYVE-1-enriched cups surrounding individual DCs (asterisks) are indicated by arrows, (**g, h**), with a digital zoomed view of an orthogonal view (**i**), (magnification: 630X, bar = 20μm). Representative images from three separate repeated experiments are shown.

Figure 8. LYVE-1 engagement with the HA coat on DCs is required for formation of transmigratory cups. (**a-c**) Quantitation of microscopy images to show numbers of LYVE-1^+ cups associating with adherent DCs in mLEC monolayers overlaid with BMDCs (**a, b**) following co-culture and incubation in the presence of anti-mouse mAbs (**a**) or following 2 h pre-incubation with hyaluronidase (HAase), (**b**) and in human LECs with MDDCs in the presence of the HA blocking mouse anti-human mAb 891 (**c**). Data represent the mean ± s.e. (n = 4) from one experiment of three. (**d**) Detection of HA on endogenous dermal DCs during transmigration into lymphatic vessels *in vivo*, in frozen skin sections from BALB/c mice subjected to

oxazolone hypersensitization. Sections were immunostained using bVG1 (blue), anti-MHCclII-FITC (green) and anti-podoplanin to identify lymphatic vessels (red), bar = 10µm. (**e**) Orthogonal view of a LYVE-1-enriched cup surrounding an individual DC, as shown in a z-stack of whole-mount mouse dermis, immunostained with rabbit anti-LYVE-1 (red), 24 h following topical application of oxazolone and intradermal injection of CMFDA-labeled BMDCs (green), magnification: 630X, bar = 20µm.

Methods

Human and animal studies

All studies using human tissue were approved by the Oxford Regional Health Committee (OXREC). Animal studies were performed with appropriate UK Home Office licenses with Oxford University ethical approval.

Lyve1$^{-/-}$ mice on C57BL/6 background were kindly provided by Regeneron Pharmaceuticals NY, USA[23]. Mice were backcrossed for 10 generations onto a BALB/c background and subsequently maintained as a heterozygous colony at Biomedical Services, John Radcliffe Hospital. F5 TCR-transgenic mice recognizing the H-2D^{b}-restricted influenza virus nucleoprotein epitope ASNENMDAM (Flu-NP$_{366-374}$) were kindly provided by Dimitris Kioussis (National Institute of Medical Research, London, U.K.) and maintained at the Biomedical Services Unit (John Radcliffe Hospital, Oxford, U.K.). C57BL/10 and C57BL/6 mice were purchased from Envigo RMS Inc, Bicester, Oxfordshire. OT-1 C57BL/6 TCR transgenic mice recognizing the H-2K^{b}-restricted ovalbumin epitope SIINFEKL were obtained from the Jackson Laboratory, Bar Harbor Maine, USA. CD11c-GFP reporter mice were a kind gift from Fiona Powrie (Kennedy Institute of Rheumatology, University of Oxford). All animal studies were performed with appropriate UK Home Office licenses and with approval of the Oxford local ethics committee.

Genotyping

Ear notches from mice generated by *Lyve1*$^{-/+}$ x *Lyve1*$^{-/+}$ breeding were digested in 200 µl DirectPCR (Tail) lysis reagent (Viagen 102-T) supplemented with Proteinase K, 0.4 mg/ml (Sigma-Aldrich P2308) for 16 h at 55 ˚C, then heated to 85 ˚C for 45 min prior to use in PCRs. MyTaq^{TM} Red Mix (Bioline) and primers at 0.8µM working concentrations were used, denaturing at 94 ˚C for 4 min initially, followed by 40 cycles of 94 ˚C for 1 min, annealing at 50 ˚C for 45 seconds and

extending at 72 ˚C for 45 seconds in a Hybaid PCR machine. 3' end genotyping PCR used the primers pGK.Neo.2Fw (K/O forward primer) TCA TTC TCA GTA TTG TTT TGC C, 3'Lyve-F3 (WT forward primer) CGT GAA AAG GTG AGG TTG, and 161 SD (Common reverse primer) TCA CTC CTA TTG AAC AGT ACC, yielding PCR products of 381 bp for the K/O band and 310 bp for the WT band. 5'end genotyping PCR used the primer 161 SU (Common forward primer) GGA GGC TTC CTT ACA TAG AC with either LACZ.SEE-RD (K/O reverse primer) GTC TGT CCT AGC TTC CTC ACT G or 5'Lyve-R2 (WT reverse primer) GAC AAA GGT TAG AAG GCA C, yielding products of either 556 bp for K/O or 554 bp for WT. Products were electrophoresed on 1.2% agarose-Tris-Borate-EDTA gels.

Antibodies

Rat anti-mouse LYVE-1 (mAb2125) was purchased from R & D Systems; mAbs B1/10 and C1/8 were generated previously, using mouse LYVE-1 Fc as immunogen[28,29], as was rabbit anti-LYVE-1 polyclonal antibody[20]. Rat IgG fractions were purified from hybridoma supernatants using Protein G-Sepharose. Other antibodies were mouse anti-human LYVE-1 (R & D Systems, clone 891) and goat anti-mouse podoplanin (R & D Systems AF3244), hamster anti-mouse podoplanin (eBioscience 14-5381-85 clone 8.1.1), rat anti-mouse CD31 (BD Pharmingen), rat anti-mouse VE-cadherin (BD Pharmingen), rat anti-mouse ICAM-1 (YN1/1.7.4) (hybridoma cultured in-house, purified using Protein G-Sepharose and as used previously in [15]. All antibodies were used at 10 µg/ml for immunostaining and 50 µg/ml for function-blocking. Biotinylated hyaluronan binding protein (bHABP, recombinant human versican G1 domain, bVG-1, AMSBio, AMS.HKD-BC41) was used at 3 µg/ml, detecting with either streptavidin-conjugated AlexaFluor 647 or streptavidin-conjugated AlexaFluor-Pacific Blue. All secondary conjugates

762 (AlexaFluor 488, 546, 594, 647) were purchased from Molecular Probes, Invitrogen.
763 Irrelevant IgG isotype controls were purchased from R & D Systems. Mouse
764 antibodies for flow cytometry were as follows: anti-CD11c-PE/Cy7 (Biolegend
765 117318 clone N418), anti-CD11b-BUV395 (BD Biosciences 563553, clone M1/70),
766 anti-MHCII (I-A/I-E)-eFluor450 (eBioscience 48-5321-82 clone M5/114.15.2), anti-
767 CD45-BV785 (Biolegend 103149 clone 30-F11), anti-EpCAM-BV605 (Biolegend
768 118227 clone G8.8), anti-Langerin-PE (eBioscience 12-2075-82 clone eBioL31, anti-
769 CD103-APC (eBioscience 17-1031-82 clone 2E7), anti-F4/80-PE/Cy5 (Biolegend
770 123112 clone BM8), and anti-CD86-PE (BD Pharmingen 553692 clone GL1). All
771 antibodies that were used for functional assays (both *in vivo* and *in vitro*) were tested
772 for endotoxin contamination using a Pierce™ LAL Chromogenic Endotoxin
773 Quantitation kit (ThermoFisher Scientific 88282), according to the manufacturer's
774 protocol, to ensure that endotoxin levels were less than 10 pg/ml.

775 ***Cells***

776 Primary mouse and human lymphatic endothelial cells (mLECs and hLECs) were
777 prepared from freshly resected skin samples by immunoselection with LYVE-1 mAb
778 and MACS® beads (Miltenyi Biotec), as described previously[15]. Bone marrow derived
779 DCs (BMDCs) were extracted from tibia and fibula bones of euthanized mice, passed
780 through a 70 µm cell strainer and cultured for 7 days in DC medium (RPMI 1640 with
781 10% FCS, kanamycin sulfate, MEM non-essential amino acids, sodium pyruvate,
782 glutamine, 2-mercaptoethanol (55 mM), (all Life Technologies), and supplemented
783 with recombinant mouse GM-CSF and IL-4 (20 ng/ml, premium grade, Miltenyi
784 Biotec). $CD11c^{+}MHCclII^{+}$ phenotype was routinely confirmed by flow cytometry
785 (**Supplementary Fig. 4a**). Human monocytes were purified from PBMCs from
786 healthy donors by positive immunoselection using anti-CD14-conjugated MACS®
787 beads (Miltenyi Biotec). DCs were generated by culturing monocytes for 5 days in

DC medium, supplemented with recombinant human GM-CSF (50 ng/ml) and 10 ng/ml IL-4 (premium grade, Miltenyi-Biotec). Non-adherent DCs were matured with 1 µg/ml LPS from *Salmonella abortus* (Sigma-Aldrich) and labeled with CMFDA Cell Tracker Green (Invitrogen), following the manufacturer's protocol. Jurkat E6.1 cells were purchased from Sigma and tested in-house to ensure that there was no mycoplasma contamination.

Migration of DCs following oxazolone sensitization and FITC painting

For measurement of endogenous dermal DC trafficking, 8 week old *Lyve1*$^{-/-}$ C57BL/6 or BALB/c mice or *Lyve1*$^{+/+}$ littermate controls were sensitized by topical application of 3% (w/v) oxazolone (4-ethoxymethylene-2 phenyl-2-oxazoline-5-one; Sigma-Aldrich E0753) + 4 mg/ml FITC (Fluorescein isothiocyanate isomer 1, Sigma-Aldrich F7250) in 95% aqueous ethanol to the shaved abdomen (150 µl/mouse). Where appropriate, anti-LYVE-1 mAbs C1/8, B1/10 or 2125 (0.5 mg/mouse) were administered by intraperitoneal (i.p) injection, 24 h prior to oxazolone and FITC painting. To assess the effects of anti-LYVE-1 mAbs on the challenge phase of contact hypersensitivity, mice were sensitized by topical application of 3% (w/v) oxazolone in 95% aqueous ethanol to both ears (50 µl/ear) on days 0 and 1, injected i.p. with mAbs on day 5, and then given a second topical application of oxazolone and FITC (0.8% oxazolone (w/v) + 4 mg/ml FITC, 150 µl/mouse) to the shaved abdomen on day 6, prior to sacrifice on day 7.

For trafficking of adoptively transferred BMDC, mice were sensitized and challenged with oxazolone to increase mobilization essentially as above, except oxazolone sensitization was applied to the abdomen rather than the ears and the CMFDA labeled BMDC (1 x 10^6) were injected intradermally at the same time as oxazolone challenge, 24h after i.p. injection of anti-LYVE-1 blocking mAbs (0.5mg/mouse) where indicated.

Ex vivo *DC crawl-out assays from mouse ear explants*

Ears were removed from naïve mice following sacrifice, then peeled into dorsal and ventral halves and either cultured for 24 h (exposed dermis-side down) in 24-well dishes in RPMI 1640 supplemented with 10% FCS, penicillin-streptomycin and glutamine (Life Technologies) and mouse TNFα, 50 ng/ml (R and D Systems). After culturing, dermal sheets were removed and digested in Collagenase P, (0.2 mg/ml; Roche 11213865001) and Dispase, 0.8 mg/ml (Life Technologies 17105-041) in RPMI at 37 ˚C for 30 min, then mechanically disrupted through a 100 µm cell strainer prior to staining alongside egressed cells for flow cytometry.

When investigating the effects of anti-anti-LYVE-1 mAbs on ability of DCs to egress from ear dermis, mAbs were administered to live naïve mice by i.p. injection (0.5 mg). 24 h later, mice were sacrificed and dermal sheets cultured in the presence of mouse TNFα, 50 ng/ml, and appropriate mAb (50 µg/ml) for a further 24 h.

Removal of surface HA from BMDCs for adoptive transfer

Non-adherent BMDCs were incubated with hyaluronidase, 15 U/ml (from *Streptomyces hyalurolyticus*, Sigma-Aldich), for 2 h at 37 ˚C in DC medium, then washed and replated in DC medium supplemented with HEPES 25 mM (Life Technologies) and 4-Methylumbelliferone (7-Hydroxy-4-methylcoumarin) Sodium Salt, 4-MU (Sigma-Aldrich M1508, 0.1 mM dissolved in ddH_2O) for 72 h. Maturation was induced by adding LPS 1 µg/ml during the final 24 h incubation. Control (untreated) BMDC were mock-treated in parallel with the hyaluronidase/4-MU treated cells. Non-adherent cells were then labeled with either Qtracker® 655 (Q25021MP) or Qtracker® 585 (Q25011MP) cell labeling kits, according to the manufacturer's protocol, then washed and mixed 1:1 prior to co-injection intradermally into the ears of oxazolone-sensitized mice, 0.5 x 10^6 cells of mock-treated and 0.5 x 10^6 cells hyaluronidase/4-MU treated per injection.

MVA.HIVA.NP-specific lymph node T-cell response model

Lymphocytes were isolated from F5 transgenic mice and labeled with 5.5 μM CFSE (Molecular Probes, Invitrogen), re-suspended in endotoxin-free PBS and injected intravenously into sex- and age-matched naïve C57BL/10 mice (2 x 10^6 cells/mouse). After 24 h, 0.5 mg of either rat IgG, mAb B1/10 or mAb C1/8 was administered by i.p. injection to these F5-BL10 chimeras. After another 24 h, chimeras were immunized with 2 x 10^6 PFU of recombinant modified vaccinia virus Ankara expressing flu-$NP_{366-374}$ (MVA.HIVA.NP), intradermally, or, in the case of controls for spleen T-cell proliferation, *via* an intravenous route. mAbs were administered again 24 h after MVA.HIVA.NP injection and mice were sacrificed a further 48 h later (i.e. 3 days after MVA.HIVA.NP vaccination). Draining cervical LNs and spleens were removed and single cell suspensions obtained in FACS incubation buffer (PBS + 1% FCS, 0.01% sodium azide), then stained for NP-specific $CD8^+$ T-cells using human influenza virus A-$NP_{366-374}$-specific tetramer (1/160 dilution)[28] and PerCP-conjugated anti-CD8α mAb (1/150 dilution, BD Biosciences). Cells were washed twice in FACS buffer then resuspended in CellFix (BD Biosciences). For analysis by flow cytometry, cells were gated according to forward-scatter, side-scatter and pulse width to obtain singlets, then by detection of CD8 and NP.

Ovalbumin-specific lymph node T-cell response model

$CD8^+$ lymphocytes were isolated from C57BL/6 OT-1 transgenic mice and purified by negative immunomagnetic bead selection (Miltenyi-Biotec), prior to labeling with 5 μM CFSE (Molecular Probes, Invitrogen). Cells were then washed in endotoxin-free PBS and injected intravenously into naïve sex- and age-matched C57BL/6 *Lyve1*$^{-/-}$ mice or *Lyve1*$^{+/+}$ littermate controls (4 x 10^6 cells/mouse). The following day, BMDCs (prepared from age- and sex-matched C57BL/6 as described above) were incubated for 1 h in the presence of ovalbumin peptide SIINFEKL (1 x 10^{-7}M) and

LPS (1 µg/ml), then washed four times in PBS and injected intradermally into the ears of the OT-1 chimeras (0.5 x 10^6 BMDCs per ear). Mice were sacrificed 44 h later; draining cervical LNs and non-draining inguinal LNs were removed, passed through 100 µm cell strainers to obtain single cell suspensions, then stained for OT-1-specific $CD8^+$ T-cells using tetrameric H-2 K^b/$OVA_{257–264}$ peptide complexes conjugated with APC, anti-CD8-BV421, anti-CD25-PerCPCy5.5 and anti-CD69-PECy7, in the presence of TruStain fcX (anti-mouse CD16/CD32 clone 93, Biolegend) Fc blocker. Finally, cells were incubated with Live-Dead near-IR dead cell stain (ThermoFisher Scientific). For analysis by flow cytometry, cells were gated according to forward- and side-scatter to obtain singlets, then by detection of live dye-excluding cells, which were further characterized by expression of CD8 and detection of ovalbumin peptide by tetramer.

Flow cytometric analysis of LNs

LNs from either naïve or topical oxazolone-hypersensitized mice were cut into halves and digested for 37 ˚C in Collagenase D (Roche 11088882001), 1 mg/ml (w/v) in RPMI 1640, then mechanically disrupted through a 100µm cell strainer. Cells were suspended in incubation buffer (PBS + 10% FCS, 0.01% azide) and maintained on ice for all subsequent incubation steps. Cells were first incubated with Fixable Viability Dye eFluor780 (eBioscience 65-0865) for 15 min, then with TruStain FcX (anti-mouse CD16/CD32 clone 93, Biolegend) Fc blocker for 15 min, prior to incubation with fluorescently conjugated antibodies for 20 min. Cells were then washed and incubated for 15 min in IC Fixation Buffer (eBioscience 00-8222-49) prior to washing in Permeabilization Buffer (eBioscience 00-8333-56) and staining using anti-Langerin-PE. Staining with recombinant biotin-labeled versican G1 domain (bVG1), (Biotinylated hyaluronic acid binding protein AMS.HKD-BC41 from AMS Biotechnology (Europe) Ltd) was carried out after all other incubations, by fixing the

cells in 2% formaldehyde (v/v) for 5 min, then incubating with bVG1, 3 µg/ml for 40 min followed by streptavidin-AlexaFluor647 (Life Technologies S21374) for 40 min.

Cells were counted either manually or using 123count eBeads (eBioscience 01-1234-42), and analyzed using a flow cytometer (either CyAn, Beckman Coulter, or LSRII, BD Biosciences) and using Flow-Jo software. Compensation was carried out using anti-mouse Ig/negative control compensation particle set beads (BD CompBeads 552843) and fluorescence-minus-one controls. As a control for non-specific binding of bVG1, samples were treated with hyaluronidase (see below) prior to immunostaining.

Immunofluorescence antibody staining of cells and tissues

Monolayers of cells cultured in 8-chamber slides (BD Falcon) were fixed in paraformaldehyde (1% w/v in PBS, pH 7.4) for 5 min, washed in PBS and then primary antibodies applied in blocking buffer (PBS + 1% BSA + 10% FCS). Cells were incubated at room temperature for 45 min, followed by washing and further incubation for 30 min with AlexaFluor secondary antibodies, prior to mounting in Vectashield+DAPI (Vector Laboratories H-1200) and viewing on a Zeiss LSM 780 confocal microscope. Images were captured by sequential scanning, with no overlap in detection of emissions from each fluorophore, using either a 10X/0.3 DIC M27 Plan-Apochromat (total magnification: 100x), or 40X/1.1 W Korr UV-Vis-IR LDC-Apochromat (total magnification: 400X), or 63X/1.4 oil Plan-Apochromat (total magnification: 630X, resolution: 0.24 µm).

For whole-mount staining, mouse dermis was fixed in 1% paraformaldehyde for 1 h, washed in PBS-Triton X-100 (0.3% v/v), blocked with BSA (1% w/v) and FCS (10% v/v) and incubated with primary antibodies at 4 ˚C overnight and fluorescently conjugated secondary antibodies at 2 h at room temperature. Tissue samples were then mounted in Vectashield (Vector Laboratories H-1000) and viewed

by confocal microscope. When staining tissue to detect transmigratory cups, tissue was left non-permeabilized, omitting Triton X-100.

For preparation of thin frozen sections, tissues were frozen in OCT Embedding Medium (R. A. Lamb Laboratory Supplies) before cutting 8 µm sections by cryostat. Primary antibodies and subsequently AlexaFluor conjugates were applied, prior to mounting in Vectashield and viewing by confocal microscope.

LEC-DC adhesion and transmigration assay

To quantify adhesion, confluent monolayers of primary mLECs in gelatin-coated 24-well dishes were layered with 5 x 10^5 fluorescently labeled LPS-matured BMDCs per well and incubated at 37 ˚C for 3 h. The total numbers of DCs present were then measured in a fluorescence plate reader, followed by gentle rinsing (three times with PBS) to remove non-adherent DCs, before re-measuring fluorescence and calculating the percentage of adherent cells. To assess the effect of LYVE-1 blocking mAbs the monolayers were pre-incubated (30 min, 37 ˚C) with LYVE-1 mAbs or control Ig as appropriate before layering with BMDCs. To remove HA from cell surfaces prior to assaying for adhesion, cells were pre-incubated with hyaluronidase, 15 U/ml (from *Streptomyces hyalurolyticus*, Sigma-Aldich), for 2 h at 37 ˚C, then washed in medium.

For measurement of transmigration, primary mLECs were seeded onto the underside of gelatin-coated Fluoroblok™ cell culture inserts (3 µm pore size, BD Falcon) and cultured in companion plates until fully confluent. Monolayers were then pre-incubated (37 ˚C, 30 min) with LYVE-1-blocking mAbs or control Ig as appropriate prior to the addition of 5 x 10^5 fluorescently labeled LPS-matured bone marrow-derived DCs per well and transmigration assays carried out as described previously[15], using a fluorescence plate reader (Synergy HT, Bio-Tek) at 37 ˚C.

943 ***Quantitation of LYVE-1$^+$ endothelial cup formation***

944 Primary mLECs were seeded in 8-chamber slides and cultured until confluent.
945 Antibodies were applied 30 min before addition of 0.1 x 10^6 fluorescently labeled
946 LPS-matured BMDCs per chamber. Cells were incubated at 37 ˚C for 3 h then non-
947 adherent DCs were removed by gentle washing with PBS, prior to immunostaining as
948 detailed above. Adherent DCs from 10 fields of view per chamber were counted and
949 scored as either alone or in association with LYVE-1$^+$ cups.

950 ***Quantitation of DC hyaluronan levels***

951 A hyaluronan ELISA kit was purchased from Echelon Biosciences and the
952 manufacturer's protocol was followed. BMDCs were prepared from three *Lyve1*$^{+/+}$
953 BALB/c mice as described above, removing non-adherent cells to fresh tissue culture
954 ware and culturing them for 24 h ± LPS, (1 µg/ml) in five replicate wells of 6-well
955 dishes. Cells were counted and then supernatants applied directly to the assay. Cells
956 were lysed (150 µl/well) in lysis buffer (50 mM Tris pH 7.5, 100 mM NaCl, 1% NP-
957 40 and 1 mM EDTA) and debris removed by centrifugation (1500 RPM, 5 min) prior
958 to application to the assay. HA concentration was expressed in ng/ml per cell.

959 ***Characterization of mLYVE-1-HA blocking mAbs and epitope mapping***

960 For quantitative receptor binding analyses, mLYVE-1 mAbs B1/10, C1/8 and
961 2125 (0-5µg/ml) were titrated individually against either soluble mLYVE-1 full-
962 ectodomain Fc fusion protein, or Jurkat T-cells lentivirally transduced with full-length
963 mouse LYVE-1 cDNA using a microtitre plate binding assay and flow cytometry
964 respectively, essentially as we described previously[13,46]. For comparison of potencies
965 in HA-binding blockade, the same mouse LYVE-1 lentivirally transduced Jurkat cells
966 were subjected to high molecular weight bHA-binding assays in the presence or
967 absence of individual mLYVE-1 mAbs (0-100µg/ml), detected with streptavidin
968 Alexa485 by flow cytometry. For epitope analyses, each mLYVE-1 mAb was titrated

against a panel of full-length mouse LYVE-1 site-directed mutants in transfected HEK 293T cells, targeting individual amino acids equivalent to those identified as HA-binding residues in human LYVE-1 Link module, with correction for variation in surface expression and quantitation by flow cytometry[30].

Analysis of HA synthase expression by RT-PCR

Total cellular RNA was isolated from LPS-matured BMDCs (RNeasy, Qiagen) and first-strand cDNA synthesis was carried out by Oligo dT priming using MMLV reverse transcriptase (Epicentre, Illumina Inc), following the manufacturers' instructions. HAS2 transcripts were amplified using the primer pair mHAS2Fwd (5-GTTTTGGTGACGACAGGCAC-3) and mHAS2Rev (5-TTCCGCCTGCCACACTTCTT-3) and MyTaq^{TM} Red Mix PCR (Bioline), denaturing at 94 ºC for 1 min, annealing at 55 ºC for 2 min and extending at 72 ºC for 2 min. Products were resolved on 1.2% agarose Tris-Borate-EDTA gels, alongside 100bp DNA ladders (New England Biolabs).

Data and statistical analyses

Data was analyzed using Excel (Microsoft) and the Mann-Whitney U test was used to compare data sets throughout this study, unless otherwise stated, using Graph Pad Prism. $P < 0.05$ was considered significant. A computer-generated model of LYVE-1 was produced using the ModWeb program (https://modbase.compbio.ucsf.edu/scgi/modweb.cgi).

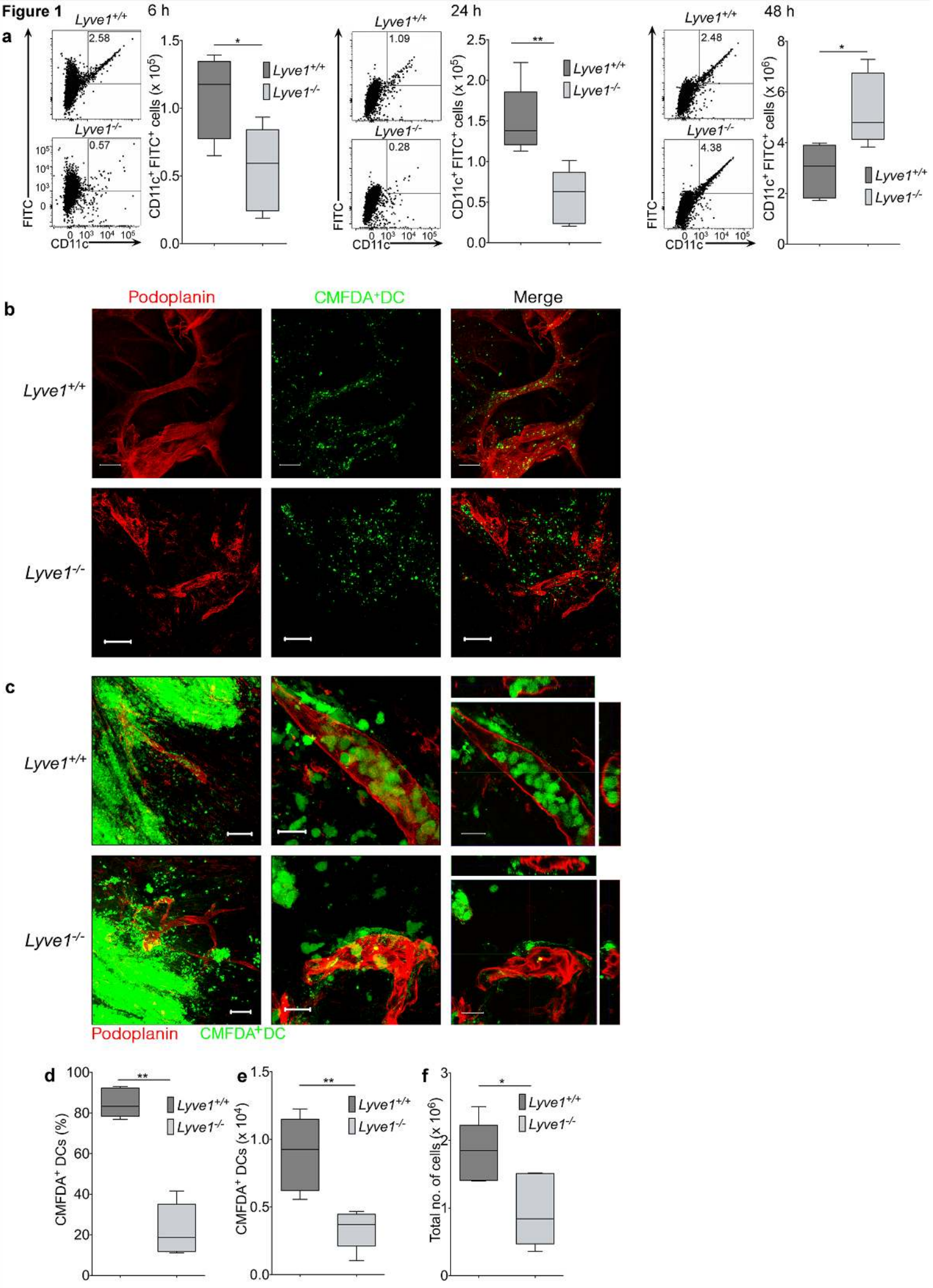
Figure 1
a
6 h
24 h
48 h
Lyve1+/+
Lyve1-/-
2.58
0.57
1.09
0.28
2.48
4.38
FITC
CD11c
CD11c+ FITC+ cells (x 10^5)
CD11c+ FITC+ cells (x 10^6)
*
**
b
Podoplanin
CMFDA+DC
Merge
c
d
CMFDA+ DCs (%)
e
CMFDA+ DCs (x 10^4)
f
Total no. of cells (x 10^6)

Figure 2

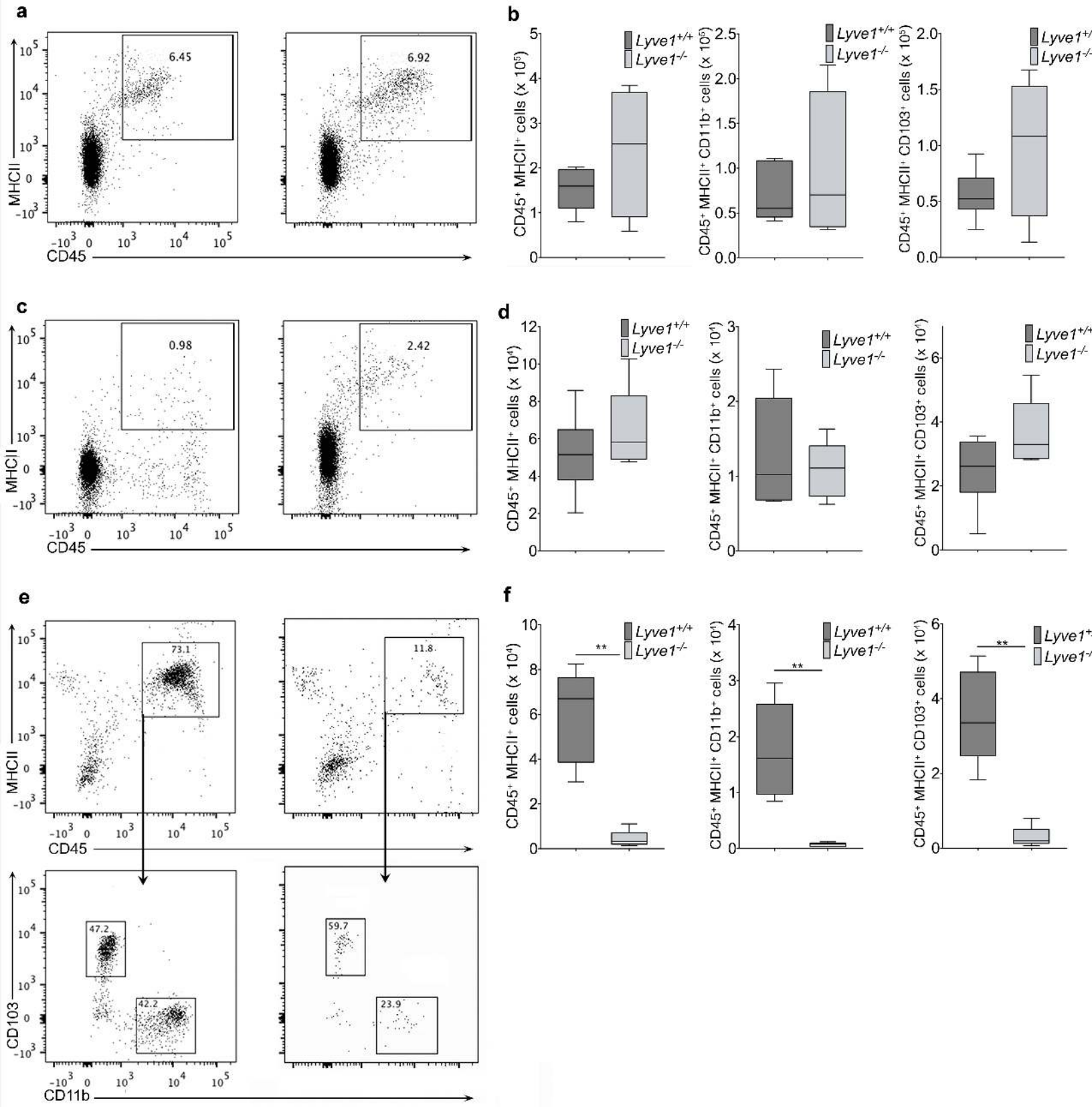
a
6.45
6.92
MHCII
CD45
b
Lyve1+/+
Lyve1-/-
CD45+ MHCII+ cells (x 10^5)
CD45+ MHCII+ CD11b+ cells (x 10^5)
CD45+ MHCII+ CD103+ cells (x 10^5)
c
0.98
2.42
MHCII
CD45
d
CD45+ MHCII+ cells (x 10^4)
CD45+ MHCII+ CD11b+ cells (x 10^4)
CD45+ MHCII+ CD103+ cells (x 10^4)
e
73.1
11.8
MHCII
CD45
47.2
42.2
59.7
23.9
CD103
CD11b
f
**
CD45+ MHCII+ cells (x 10^4)
CD45+ MHCII+ CD11b+ cells (x 10^4)
CD45+ MHCII+ CD103+ cells (x 10^4)

Figure 3

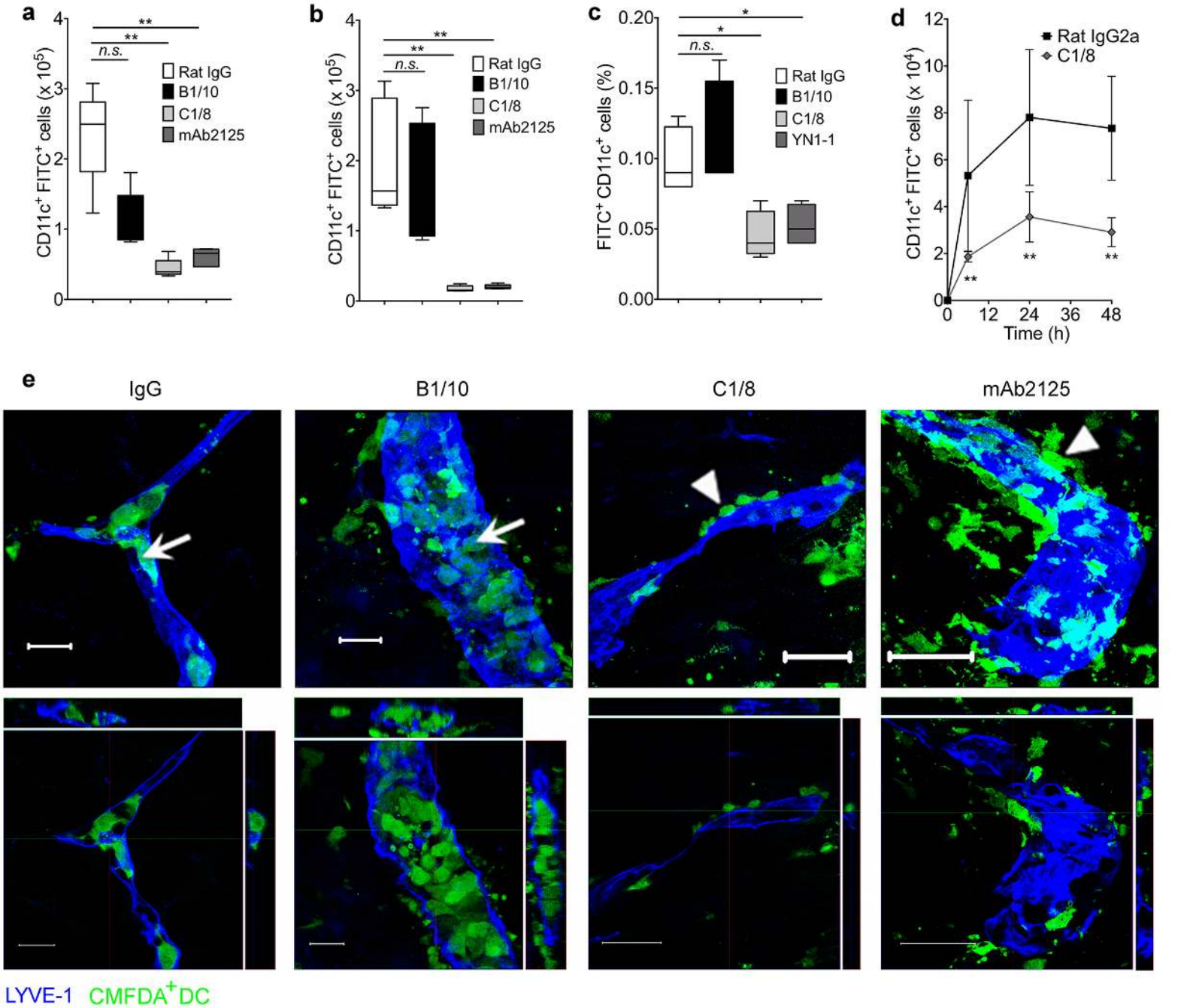
a
CD11c+ FITC+ cells (x 10^5)
n.s.
**
**
Rat IgG
B1/10
C1/8
mAb2125
b
CD11c+ FITC+ cells (x 10^5)
n.s.
**
**
Rat IgG
B1/10
C1/8
mAb2125
c
FITC+ CD11c+ cells (%)
n.s.
*
*
Rat IgG
B1/10
C1/8
YN1-1
d
CD11c+ FITC+ cells (x 10^4)
Rat IgG2a
C1/8
**
**
**
Time (h)
e
IgG
B1/10
C1/8
mAb2125
LYVE-1 CMFDA+DC
f
CMFDA+ DCs (%)
n.s.
**
**
Rat IgG
B1/10
C1/8
mAb2125
g
CMFDA+ DCs (x 10^3)
n.s.
**
**
Rat IgG
B1/10
C1/8
mAb2125
h
CD45+ MHCII+ cells (x 10^3)
n.s.
*
*
Rat IgG
B1/10
C1/8
mAb2125
i
CD45+ MHCII+ cells (x 10^4)
n.s.
*
*
Rat IgG
B1/10
C1/8
mAb2125

Figure 4

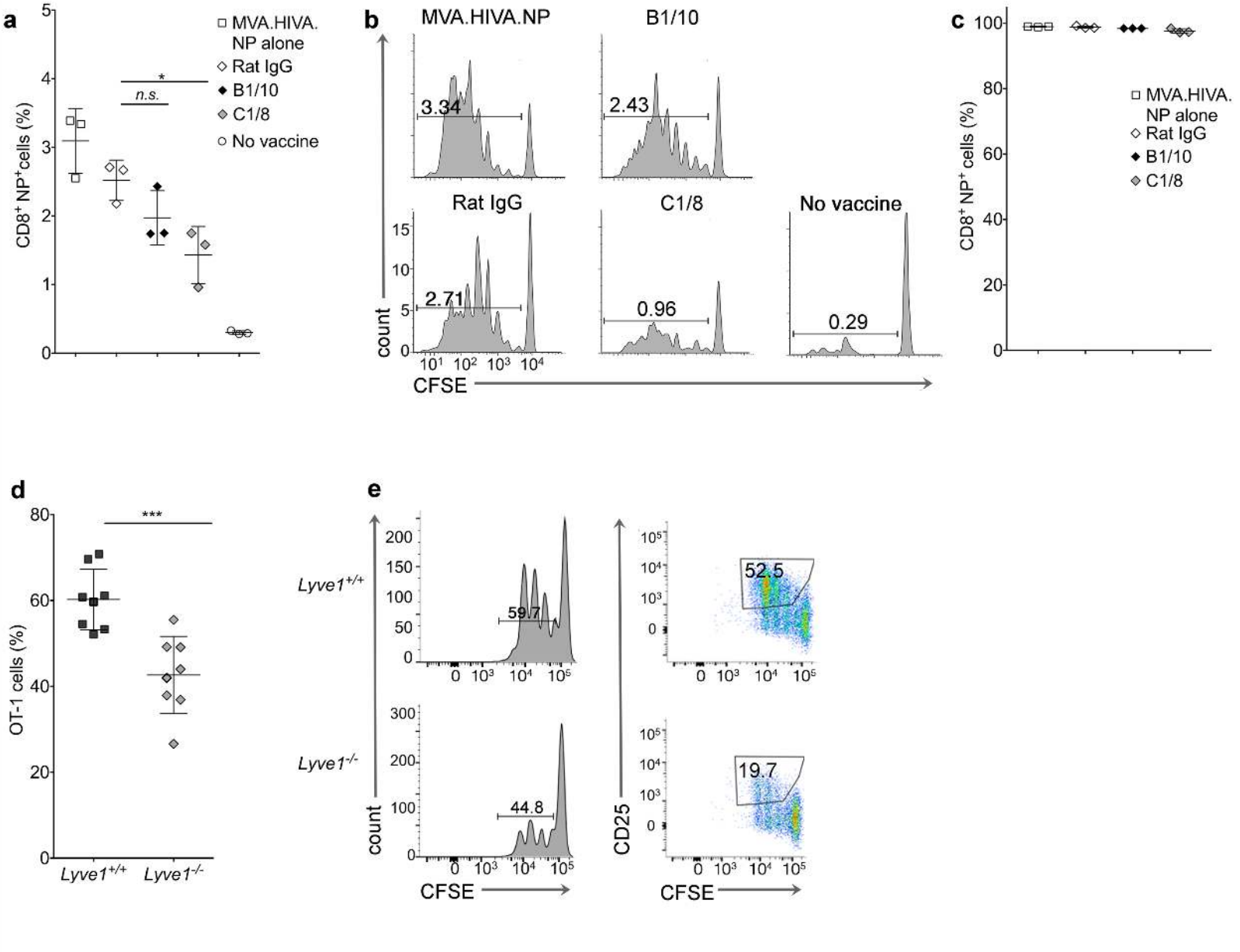
a
CD8+ NP+cells (%)
MVA.HIVA. NP alone
Rat IgG
B1/10
C1/8
No vaccine
*
n.s.
b
MVA.HIVA.NP
B1/10
Rat IgG
C1/8
No vaccine
3.34
2.43
2.71
0.96
0.29
count
CFSE
c
CD8+ NP+ cells (%)
d
OT-1 cells (%)
***
Lyve1+/+
Lyve1-/-
e
Lyve1+/+
Lyve1-/-
59.7
44.8
52.5
19.7
count
CD25
CFSE

Figure 5

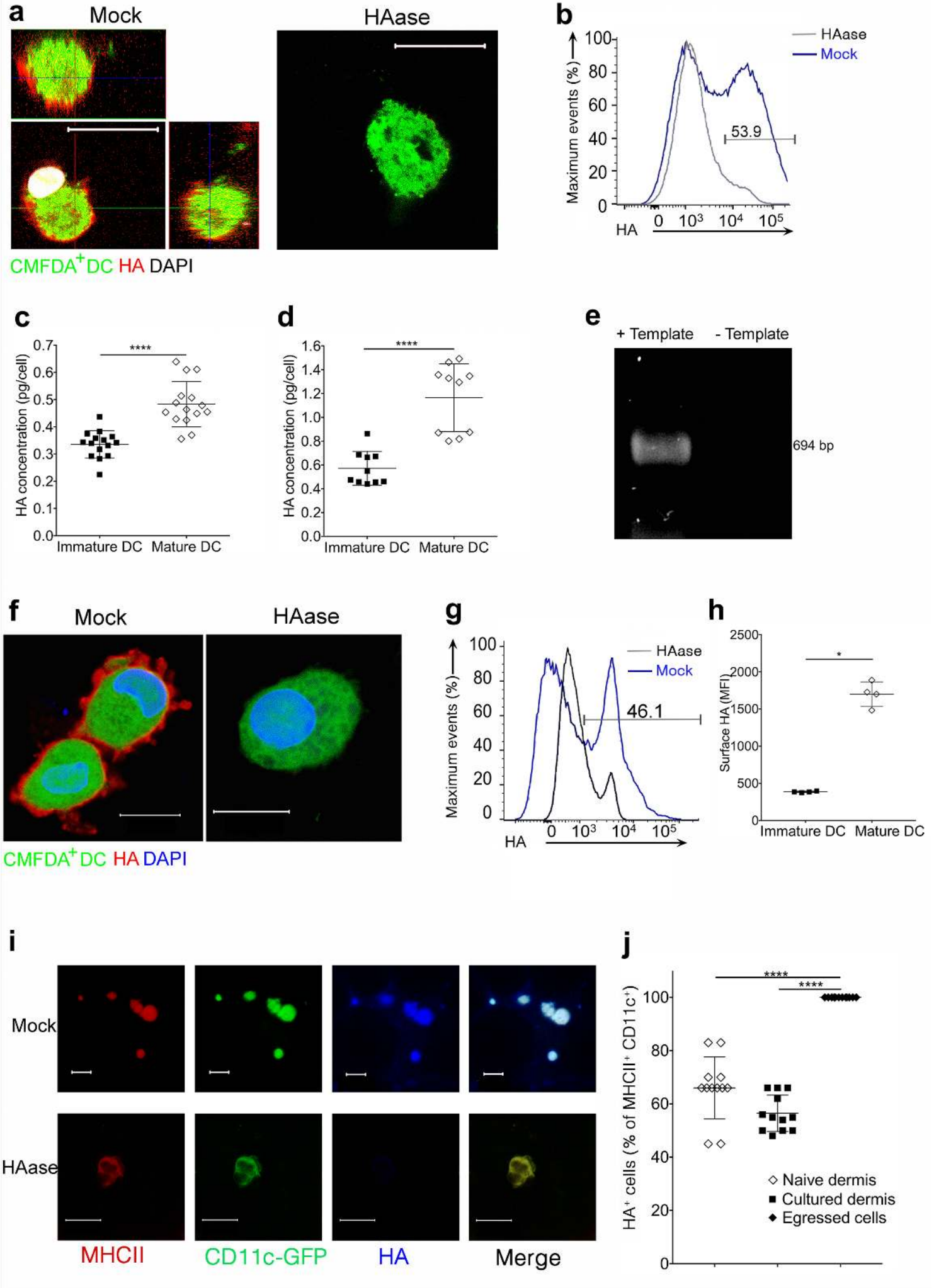
a
Mock
HAase
CMFDA+DC HA DAPI
b
HAase
Mock
Maximum events (%)
53.9
HA
c
HA concentration (pg/cell)
****
Immature DC
Mature DC
d
HA concentration (pg/cell)
****
Immature DC
Mature DC
e
+ Template
- Template
694 bp
f
Mock
HAase
CMFDA+DC HA DAPI
g
HAase
Mock
Maximum events (%)
46.1
HA
h
Surface HA (MFI)
*
Immature DC
Mature DC
i
Mock
HAase
MHCII
CD11c-GFP
HA
Merge
j
HA+ cells (% of MHCII+ CD11c+)
****
****
Naive dermis
Cultured dermis
Egressed cells

Figure 6

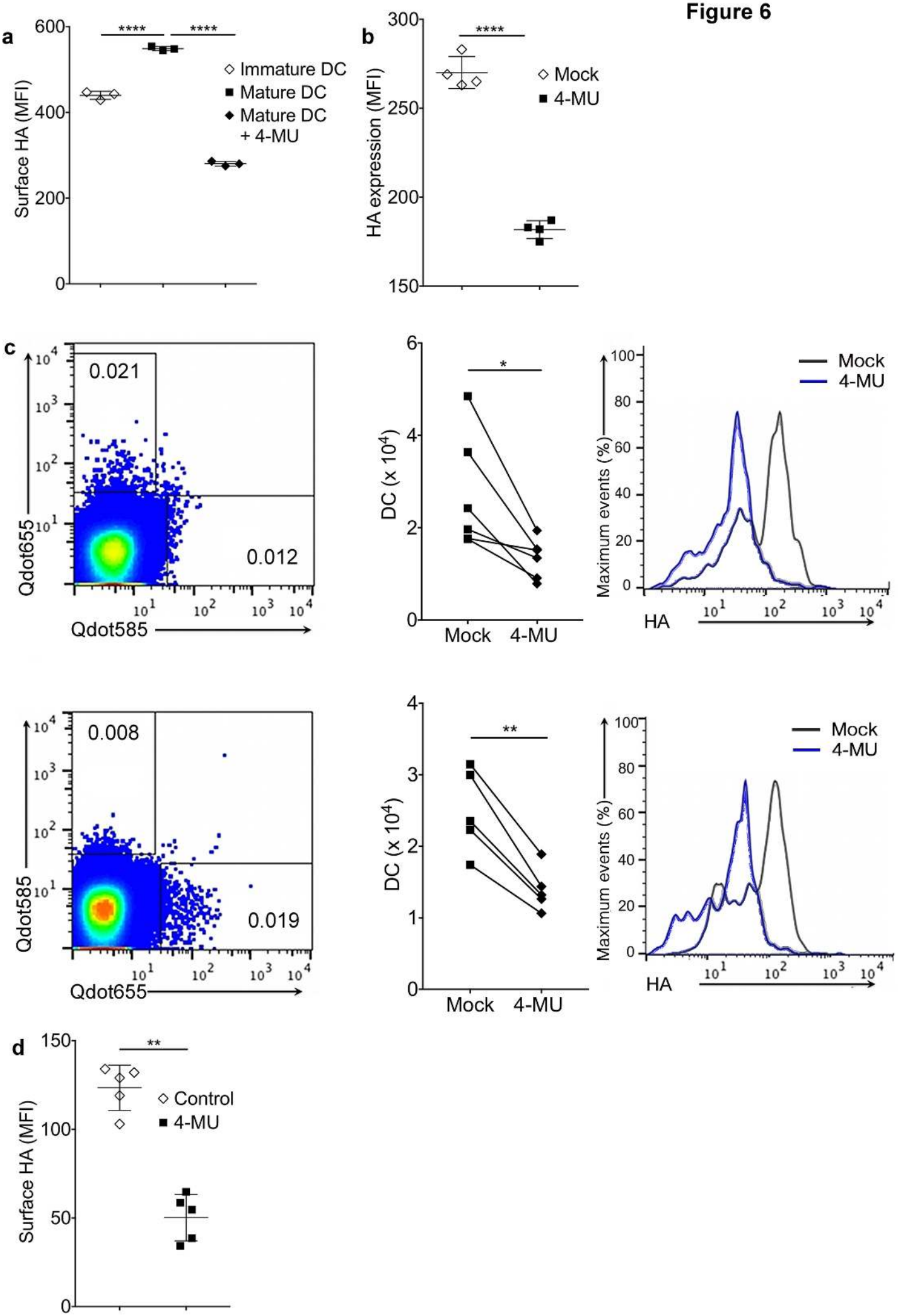
a
Surface HA (MFI)
600
400
200
0
****
****
Immature DC
Mature DC
Mature DC + 4-MU
b
HA expression (MFI)
300
250
200
150
****
Mock
4-MU
c
0.021
0.012
Qdot655
Qdot585
DC (x 10^4)
6
4
2
0
*
Mock
4-MU
Maximum events (%)
100
80
60
40
20
0
HA
Mock
4-MU
0.008
0.019
Qdot585
Qdot655
DC (x 10^4)
4
3
2
1
0
**
Mock
4-MU
Maximum events (%)
HA
Mock
4-MU
d
Surface HA (MFI)
150
100
50
0
**
Control
4-MU

Figure 7

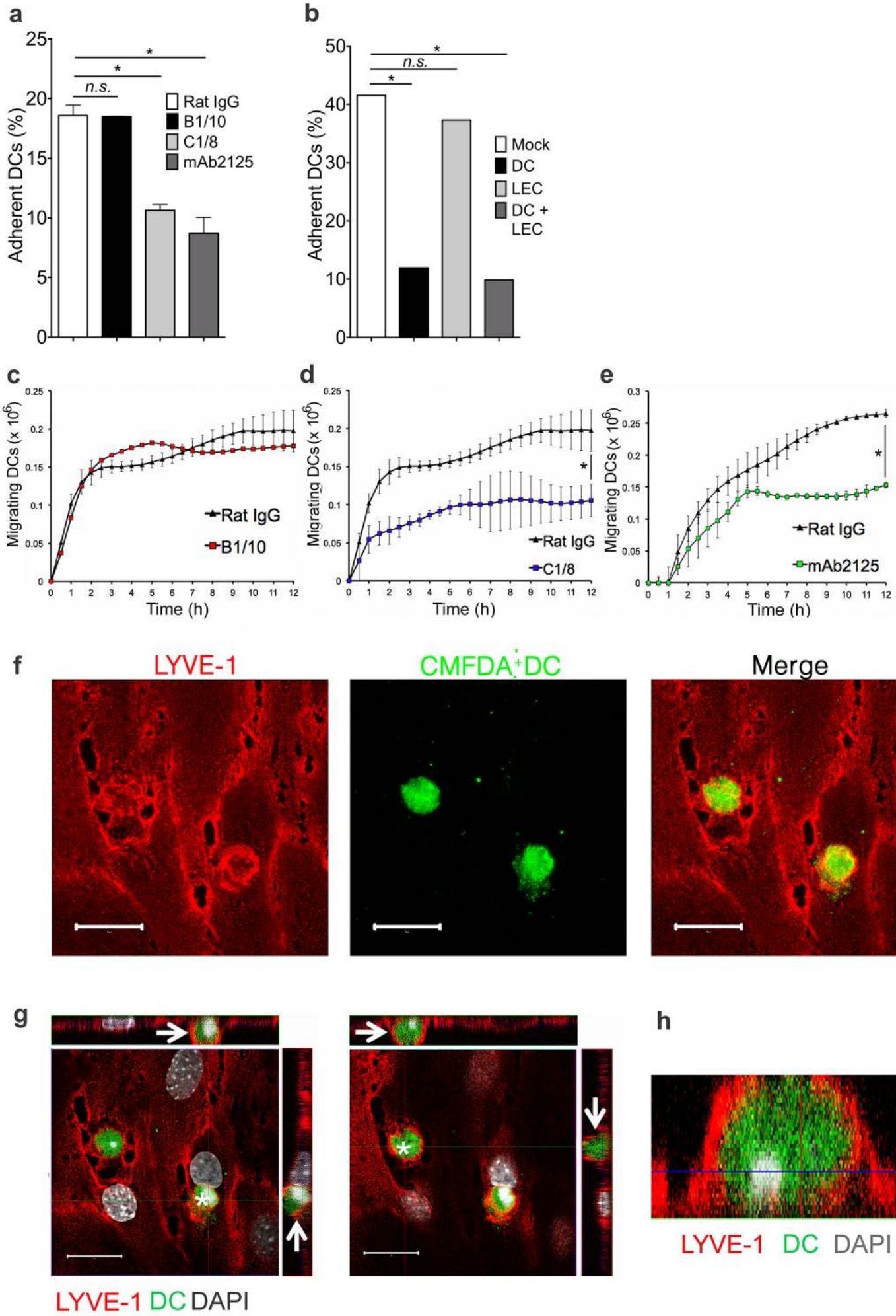
a
Adherent DCs (%)
n.s.
*
*
Rat IgG
B1/10
C1/8
mAb2125
b
Adherent DCs (%)
n.s.
*
*
Mock
DC
LEC
DC + LEC
c
Migrating DCs (x 10^6)
Time (h)
Rat IgG
B1/10
d
Migrating DCs (x 10^6)
Time (h)
*
Rat IgG
C1/8
e
Migrating DCs (x 10^6)
Time (h)
*
Rat IgG
mAb2125
f
LYVE-1
CMFDA+DC
Merge
g
LYVE-1 DC DAPI
h
LYVE-1 DC DAPI

Figure 8

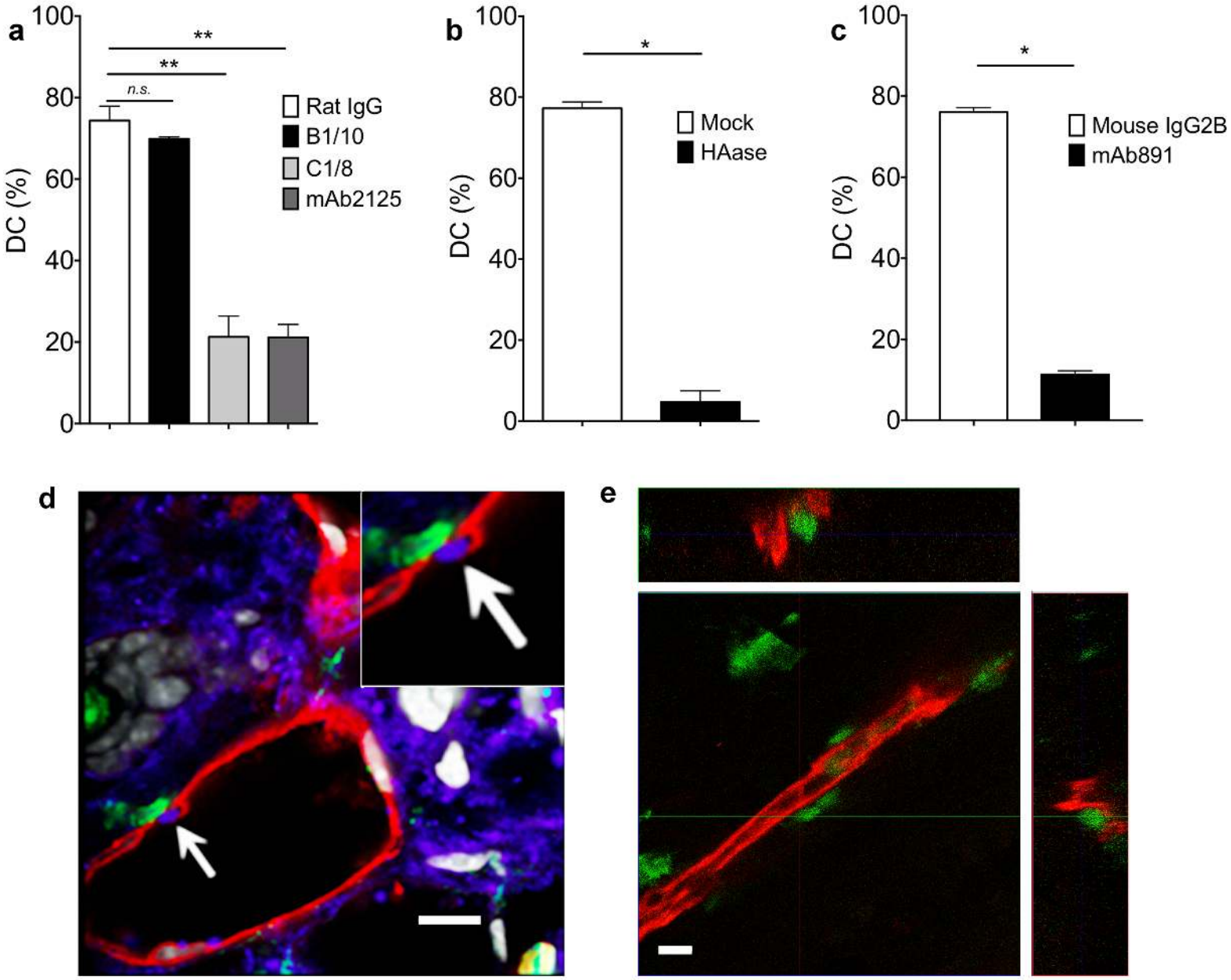
a
b
c
d
e
DC (%)
100
80
60
40
20
0
**
**
n.s.
Rat IgG
B1/10
C1/8
mAb2125
*
Mock
HAase
*
Mouse IgG2B
mAb891